Wesleyan University The Honors College

# Dynamic Vortex Drag

by

Nick Jackson

Class of 2011

A thesis submitted to the
faculty of Wesleyan University
in partial fulfillment of the requirements for the
Degree of Bachelor of Arts
with Departmental Honors in Physics

Middletown, Connecticut April, 2011

# Abstract:

This thesis explores the concept of dynamic vortex drag resulting from Kelvin wave excitations on vortex cores in thin films of superfluid $^4$He. In this system, vortex drag is commonly accepted as a significant mechanism for the dissipation of third sound wave motion; however, current models implementing a static drag force have been unable to quantitatively explain anomalous third sound free decay results found in the literature. In this thesis, many possible manifestations of Kelvin wave agitation are explored and are shown to correct the deficiencies of existing static drag theories. It is therefore concluded that vortex drag in thin films of superfluid $^4$He is most likely a dynamic, and not a static, process.

# Acknowledgements:

I would like to extend my gratitude to the Wesleyan University Physics Department for teaching me the physics that is at the backbone of this project and will underpin my development as a scientist in the years to come. In particular, I would like to thank Professor Fred Ellis for his support and encouragement in pursuing this project, his general academic and life advice during my time as an undergraduate, and his dedication towards encouraging an appreciation of dynamic climates in a southern Californian. I would also like to thank Professor Brian Stewart for inculcating an interest in sustainability, renewable energy, and broader energy/resource issues that I will carry with me throughout graduate school and the rest of my life.

Additionally, I would like to thank the Wesleyan University Financial Aid Department for their generosity and thoughtfulness in my family's times of need.

# Contents

# Ch. 1 Introduction

## 1.1 Overview

This thesis seeks to explain anomalous third sound free decay data previously taken by the Quantum Fluids Group at Wesleyan University. It will attempt to further knowledge about the mechanism of pinned vortex drag in third sound dissipation processes.

**Format:**

1. Chapter 1 will provide a brief introduction to the physics of superfluids, quantized vortices, third sound, and wave motion present on quantized vortex cores. It will also provide examples of anomalous free decays and discuss previous attempts at solving the problem that we concern ourselves with.
2. Chapter 2 will propose and implement a model used to describe the dynamic interaction of a quantized vortex tip with the resonator substrate. The model will be able to qualitatively demonstrate many of the characteristics we desire, but will ultimately fail in its rigor and completeness.
3. Chapter 3 will derive the pinning force (critical velocity) associated with a straight vortex moving over an arbitrary three dimensional resonator surface.
4. Chapter 4 will propose and implement a more rigorous quantitative model for dynamic vortex interaction with the substrate that will be seen to be capable of explaining previously unreconcilable experimental free decay data.

5. Chapter 5 will summarize the important conclusions of this thesis and identify future work that is necessary to further verify the proposal that dynamic vortex drag is an important physical phenomenon in thin-film superfluid $^4$He systems.

## 1.2 Superfluids

When the temperature of $^4$He is lowered below its $\lambda$ point of 2.17 K, the $^4$He atoms (Bosons) collapse into a macroscopic quantum-mechanical state, forming a novel state of matter known as the superfluid. Since the behavior of $^4$He atoms below the $\lambda$ point is dominated by their shared quantum-mechanical state, which overcomes any interatomic interactions, the superfluid state allows one the ability to experiment on a macroscopic quantum-mechanical system. Below the $\lambda$ point of $^4$He, the resulting superfluid system can be modeled as consisting of two distinct fluid components: the superfluid and the normal fluid. The superfluid component, as a result of being in a macroscopic quantum-mechanical state, exhibits interesting physical properties such as zero viscosity and infinite thermal conductivity. The normal fluid component can be qualitatively conceived of as a soup of thermal excitations. Within this model, each of the two components possesses its own velocity at each point within the fluid, as well as its own fraction of the system's mass density. While it is often useful to think of the superfluid system in the terms of this "two-fluid model", it is important to note that the system itself does not physically separate into two fluids, and that the utility of this model lies in its ability to facilitate conceptualization of the observed physical properties of the superfluid. All experiments referred to in this thesis were performed at temperatures below 1 K, ensuring that the thin-film $^4$He system was dominated by the superfluid component, and that the normal fluid component was negligible [1].

## 1.3 Third Sound and Free Decays

A property of superfluid $^4$He that is useful to note is its ability to be uniformly adsorbed as a very thin film over the surface of a container. These thin films possess the ability to propagate waves of many types through them. For our particular purposes, the most important type of wave that superfluid thin films can propagate is the wave type known as "third sound" [1]. Third sound waves can be thought of as the molecular analog of shallow water waves, sloshing back and forth and oscillating in a predominantly longitudinal manner. Continuing with the shallow water wave analogy, there must be a downward restoring force that allows these waves to propagate. In the shallow water wave scenario, this restoring force is the earth's gravitational force upon the ocean. Clearly, at the molecular level gravity is negligible, so the Van Der Waals force with the substrate (Au plated $SiO_2$) turns out to be the dominant restoring force in the system. In the superfluid system, the normal fluid component becomes clamped to the substrate via the scattering of thermal excitations; that is, its local velocity, $\overrightarrow{v_n}$, is zero everywhere within the film. It should be noted that the longitudinal displacement of the superfluid in third sound oscillations far exceeds its vertical displacement, thereby allowing the superfluid to be treated as an essentially two-dimensional system, greatly simplifying the required fluid mechanics.

The experiments performed by the Quantum Fluids Group at Wesleyan University, and with which we concern ourselves at present, involved electrostatically driving a resonator cavity containing a thin film of superfluid $^4$He uniformly adsorbed over the resonator surface. Third sound wave motion was driven up to a particular amplitude, and then allowed to decay away when the driving force was turned off. How these third sound oscillations decayed was then studied. At first thought, one would expect these third sound waves to experience an exponential decay as a result of thermal oscillations in the superfluid resulting from

the relative motion of the superfluid component and the normal component. On a semi-log plot, such an exponential decay would appear as a straight line, with a linear decay constant, Q. While many of the free decays can be described by this simple exponential decay model, a significant number of them exhibit anomalous behavior.

In studies performed by Anand Swaminathan '09, these anomalous free decay curves were catalogued and analyzed [2]. In his work, he found that there were two types of anomalous free decays observed: the "kink-type" (Figure 1.1) and the "bulge-type" (Figure 1.2).

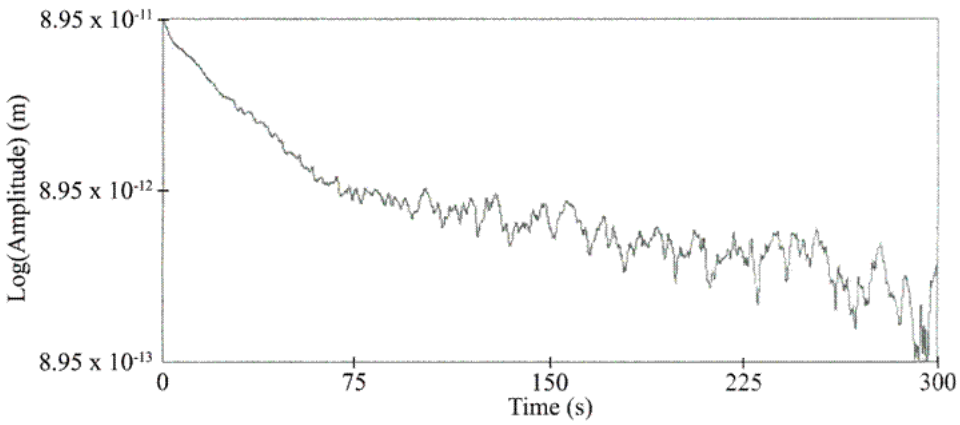


Figure 1.1 An example of a free decay exhibiting the two decay constant "kink-like" behavior on a semi-logarithmic plot.

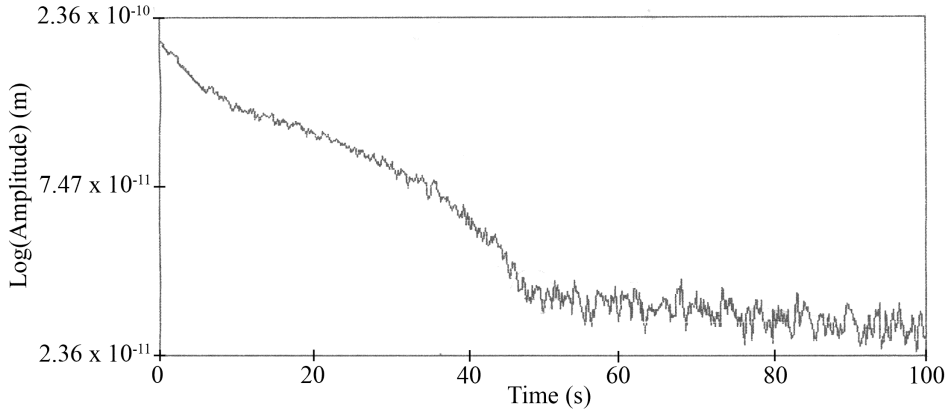


Figure 1.2 An example of a free decay exhibiting the "bulge-like" transition behavior between decay constants on a semi-logarithmic plot.

The primary purpose of the work performed by Anand Swaminathan was to identify quantized vortex motion as the mechanism responsible for the deviations from the expected simple exponential decay behavior. Ultimately, Swaminathan did not manage to completely resolve the issues behind the mechanism in these anomalous free decays; his model was able to explain the bumps, but not in a quantitatively consistent fashion. The conclusion of Swaminathan's thesis held that quantized vortex motion is still the dominant mechanism responsible for these kinds of anomalous free decay curves, however the exact dynamics of these vortices are still poorly understood. It is this issue that we will try to resolve in the following chapters, but first we must become familiarized with the general physics of quantized vortices prior to discussing their drag behavior.

## 1.4 Superfluid Vortices

All superfluid vortices can be characterized by a quantized circular flow with closed streamlines around a vortex core. This quantized circulation, $\kappa$, is simply the quantized version of the Kelvin circulation constant of classical fluid dynamics:

$$\kappa = \oint \overrightarrow{v_s} \cdot \overrightarrow{dl} = n\frac{h}{m_4} \tag{1.1}$$

where $\overrightarrow{v_s}$ is the velocity of the superfluid, $h$ is Planck's constant, $m_4$ is the mass of a $^4$He atom, and $n$ is a positive integer representing a specific quantized state of circulation [3]. Equivalently, the velocity field of a straight, quantized vortex can be expressed in the same manner as a classical vortex, except that it also carries along the quantization condition in its velocity field:

$$\overrightarrow{v} = n\frac{h}{m_4 r}\hat{\phi} \tag{1.2}$$

where $r$ is the distance from the center of the vortex [3]. The unit vector $\hat{\phi}$ denotes the direction of rotation (circulation), where positive $\phi$ implies a right-handed rotation when viewing the vortices from above. Clearly, by glancing at Equation 1.2, one can see that there is a singularity as $r \to 0$, *i.e.* inside of the vortex core. Little is known about the nature of the interior of a vortex core except that it is a region where anomalous behavior occurs. Therefore, Equation 1.2 can only be valid up to the core radius $a_0$. For superfluid vortices in $^4$He, the core radius has been experimentally measured as approximately $a_0 = 1.3$ Å [3].

Regarding the quantum number $n$ appearing in Equations 1.1 and 1.2, superfluid vortices with $n > 1$ are never seen experimentally. The reason for this lies in the energetic favorability of a single $n > 1$ vortex to break up into two vortices of $n = 1$, as a single vortex of $n > 1$ represents a higher energy state than a pair of singly-quantized vortices.

Continuing the analogy with classical vortices, a quantized vortex can be considered as a physical object due to its inherent quantum stability, and when exposed to a perturbing flow it experiences a lateral force known as the Magnus force [3]. The Magnus force arises when the rotational flow of the vortex interacts with a perturbing fluid flow. Due to the rotation of the vortex, the flow velocity on one side of the vortex will be greater than the flow velocity on the opposite

side of the vortex, resulting in a Bernoulli pressure difference on opposite sides of the vortex. In our particular case, the oscillating third sound flow acts as this perturbing flow source that the quantized vortex encounters, and it consequently induces a Magnus force that must be taken into account in the vortex's resultant motion.

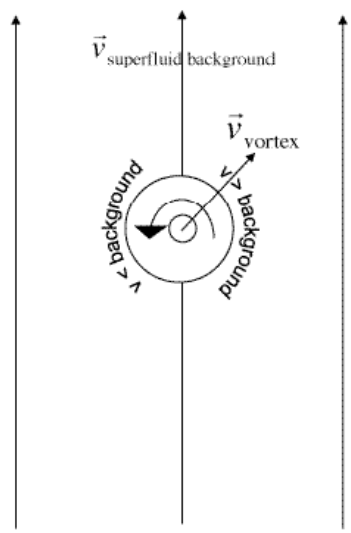


Figure 1.3 Illustration of the Magnus force on a vortex.

The Magnus force associated with a vortex that moves at a velocity $\overrightarrow{v_v}$ is given by [3]:

$$\overrightarrow{F_{Magnus}} = \rho\kappa h_0(\overrightarrow{v_s} - \overrightarrow{v_v}) \times \hat{k} \tag{1.3}$$

where $\rho$ is the density of $^4$He, $h_0$ is the length of the vortex core (height of the thin-film), and $\overrightarrow{v_s}$ is the background third sound flow at any given time in a third sound oscillation.

Another important aspect of superfluid vortices is their ability to pin to defect sites on a substrate. In early attempts to explain the "bulge-like" anomalous free decays, Fred Ellis and Hai Luo posited that the critical velocity phenomena

observed in free decays were the result of the pinning and unpinning of quantized vortices from the resonator substrate. In this first and simplest model, vortices were assumed to be pinned to surface roughness or defects (local energy minima) up to the point that a critical third sound flow velocity, $v_c$, was reached. At this point, the third sound flow would become strong enough that the Magnus force exerted on the vortex core would be sufficient to depin the vortex from the defect site, setting it free to drag along the surface of the substrate, with the critical force dissipating energy in a manner akin to a classical frictional force. When the oscillating third sound flow then decreased below this critical velocity, the vortex would repin to the nearest defect site, and the process would repeat itself at the beginning of the next third sound cycle.

It should be noted that this simple static drag force model can be used to succesfully explain energy loss in high amplitude flows [4], and is also qualitatively capable of explaining the presence of the "bulge" in the anomalous free decays [2]. However, as mentioned previously, one cannot arrive at quantitatively accurate explanations of the bulge behavior by invoking just a simple static drag force.

In order to understand the power dissipated by a vortex undergoing a static drag force, one needs to precisely understand the resulting motion of a vortex given the sum of the forces acting upon it. While vortices may be treated like objects due to the extent of their cores, the common theoretical assumption is that a superfluid vortex core possesses no mass, and therefore cannot have any net force exerted upon it, lest it feel an infinite acceleration. Using Newton's Second Law, and balancing all of the forces acting on a vortex core:

$$\overrightarrow{F_v} = \rho\kappa h(\overrightarrow{v_s} - \overrightarrow{v_s}) \times \hat{k} - f_0\hat{v}_v = 0, \tag{1.4}$$

where $f_0$ is the frictional drag force that acts in the direction opposite to the vortex's motion, one can derive the components of the vortex velocity perpendic-

ular and parallel to the third sound flow in the steady state [2]:

$$\begin{bmatrix} v_{v\parallel} \\ v_{v\perp} \end{bmatrix} = \begin{cases} \begin{bmatrix} 1-\left(\frac{v_c}{|\mathbf{v_s}|}\right)^2 \\ \left(\frac{v_c}{|\mathbf{v_s}|}\right)\sqrt{1-\left(\frac{v_c}{|\mathbf{v_s}|}\right)^2} \end{bmatrix} |\mathbf{v_s}| & \begin{matrix} v_s > v_c \\ v_s < v_c \end{matrix} \\ \begin{bmatrix} 0 \\ 0 \end{bmatrix} \end{cases} \tag{1.5}$$

One must keep in mind that Equation 1.5 is only valid for a static drag force.

Since past simulations involving this static drag force model have failed at quantitatively describing many experimental phenomena, we seek to modify the vortex dynamics so that behavior other than just a static drag force is observed. The question of how one can physically argue that a vortex will experience something other than a static drag force is then the next concern that must be addressed. We propose that the dragging of the vortex across the resonator substrate does not simply dissipate energy, but also makes the vortex less likely to repin to the substrate. The simplest way to think of this argument is by imagining the drag force acting as a perturbation on the vortex tip that generates wave disturbances that propagate up the vortex core. This wave agitation results in an additional nonzero kinetic energy on the core, which can, in many conceivable ways, make it much more difficult for the vortex to repin to a defect site. This mode of thinking would then result in the drag force being decreased as a result of the dragging process, and transform the static drag model of vortex motion into one involving a dynamic drag force. The next logical step in this approach is to describe the wave motions that will be present on a quantized vortex core so that we may speak quantitatively about the amount of additional kinetic energy that would be created, and retained, on the core by such a disturbance.

## 1.5 Kelvin Waves

There are a number of wave types that have the ability to propagate on a vortex core. The most studied, and arguably most common type of wave present on a classical vortex core is the Kelvin wave. While the theory of Kelvin waves was originally formulated for a classical vortex core, Kelvin wave modes have been experimentally observed in bulk $^4$He [6]. It is reasonable to assume that vortices in the thin-film setup are also capable of propagating Kelvin wave modes on their cores.

In 1880, Lord Kelvin derived the dispersion relation for waves on a vortex core, of which there are two branches: a slow branch and a fast branch [3,7,8] . The two branches obey the following dispersion relation:

$$\omega^{\pm}(k) = \frac{\kappa}{2\pi a}\left(-1 \mp \sqrt{1 + (ka)\frac{K_0(ka)}{K_1(ka)}}\right) \tag{1.6}$$

where $K_n$ is a modified Bessel Function of order "n".

Here $(+)$ denotes the fast branch with waves moving with the circulation of the vortex, $(-)$ denotes the slow branch moving opposite the circulation of the vortex, $a$ is the core radius, and $\kappa$ is the quantized circulation constant.

It is important to both qualitatively, and quantitatively, understand the contribution that each branch provides to the total vortex wave motion. In 1985, a seminal paper on quantized vortex motion in superfluid $^4$He was published by K.W. Schwarz [5], in which he advanced much of the understanding of quantized vortex motion to where it stands today. The most important contribution made with regard to our present work is his description of vortices following the local induction approximation. In the local induction approximation, one can determine the time-evolved motion of a vortex core based purely on its geometry at a given point in time; no knowledge is needed about the velocity field. In other

words, if one were to distort a vortex core into an initial configuration, let go, and then watch the distortion propagate into time-evolved vortex motion, one could describe the subsequent motion through an understanding of only the self-interaction of the vortex with its own flow field.

In analyzing the two branches of the dispersion relation, one discovers that the fast branch does not in fact follow the self-induced local velocity field, whereas the slow branch does. Therefore, it has been common in the literature to only take interest in the slow branch [3]. It is also true that the fast branch motion happens on much faster time scales than that of the slow branch, and therefore is not of as much interest for the description of slow vortex-flow interactions in our present discussion [3,5].

However, one cannot simply throw away the fast branch without understanding the effects of that action. In the Schwarz paper, Schwarz shows that one can effectively linearize the equations of motion for vortex self-interaction and time propagation and get dynamics that are consistent with solving the exact equations of motion. In throwing away the fast branch, one does, however, lose some information. In our own studies, we linearize the equations of motion and use Fourier analysis to understand the effect of discarding the fast branch of the dispersion relation. Ultimately, we learn that when one uses only the slow branch, one cannot completely specify the position and velocity of the vortex core simultaneously. The local induction approximation is an entirely deterministic method depending solely on the vortex geometry, and when used, one cannot control the velocity field of the vortex. Therefore, we only specify the geometry of the vortex in our simulations.

In order to check that linearized Fourier analysis is an adequate means of describing Kelvin wave propagation on a vortex core, we performed simulations involving the time evolution of geometrical distortions on the core. In Figure 1.4, snapshots in time of a representative simulation are presented. In this simulation,

an initial Gaussian disturbance is set on an infinite vortex core, and the motion is propagated through time using linear Fourier analysis. If at any point in time one imagines a right handed circulation, curls his/her right hand around the core in the direction of that circulation, and then imagines his/her fingers as the flow of the vortex, one can see that this flow, through self-interaction with the rest of the vortex core, can be used to predict the frame by frame progression of the vortex's geometry. The last frame of Figure 1.4 is simply provided to show that after long times, the disturbance has effectively propagated away from the initial distortion site.

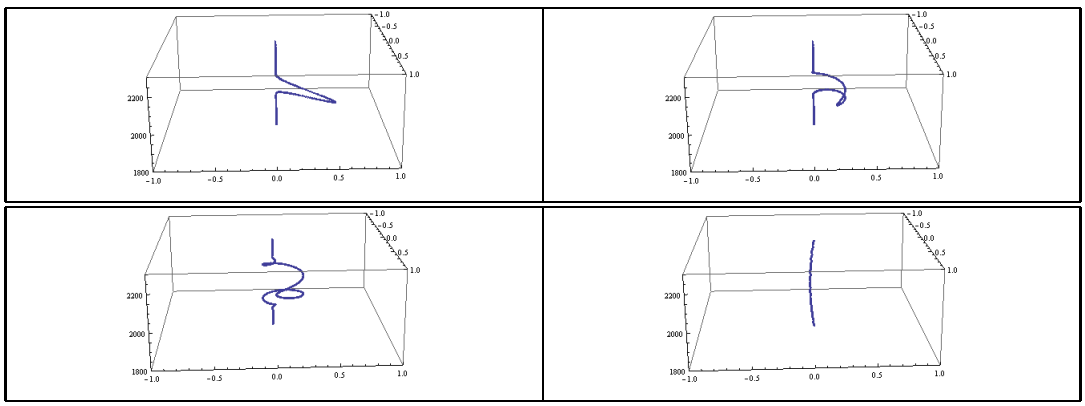

Figure 1.4 - Time propagation of Kelvin waves on a vortex core resulting from an initial Gaussian displacement. Propagation times are scaled to the core frequency. Top left: $t = 0$. Top right: $t = 5$. Bottom Left: $t = 10$. Bottom Right: $t = 100$.

It is important to note that this Fourier linearization of the wave motion results in behavior that is consistent with the Schwarz model, as that is the seminal paper for understanding such vortex motion. In performing these simulations, we learn that we have an understanding of this slow branch of vortex motion. However, it must be remembered that we can still only specify the position of the vortex; the velocity field cannot be independently controlled. Another important question to ask, however, is how will our linearized model, which only considers the slow branch, respond to an arbitrary boundary condition in time?

Since we are ultimately concerned with the dragging of the vortex tip across the substrate, which will produce wave agitation on the core, we proceeded by invoking multiple boundary conditions in time for the vortex tip and trying to control one, and then two dimensions of the vortex tip motion, again using linear Fourier analysis. What we learned from these simulations is that one may control only one dimension of motion at a time. The other dimension of motion is required to be free in order for the vortex to deal with the repercussions of the motion being controlled in a single dimension; if the x-component of the vortex tip is controlled, then the y-component must be free in order to deal with the x-component manipulation, lest no solution exist at all. We performed simulations for sawtooth, Gaussian, triangle, and square waves in one dimension of motion using linearized Fourier analysis on the slow branch of the dispersion relation, and observed behavior that is consistent with what we expect from the Schwarz model. This exercise was useful because it demonstrated that a time-dependent disturbance at the vortex tip is indeed capable of propagating Kelvin waves up the core that we may understand using the local induction approximation and linear Fourier analysis. If one needs to know the exact behavior of the uncontrolled dimension of motion, it can be analytically solved for, resulting in Equation 1.7 provided below (See Appendix A for derivation):

Given some x(t), the resulting y(t) is given by:

$$y(t) = \lim_{\lambda \to 0} \frac{1}{\pi} \int_{-\infty}^{\infty} x(t-s) \frac{s}{s^2+\lambda^2} ds \tag{1.7}$$

Lastly, since we will eventually be looking to these Kelvin waves as a means of understanding energy dissipation in our system, it is important to understand just how much energy is associated with a vortex that has been distorted from equilibrium. This result has already been formulated in papers addressing Kelvin waves in bulk $^4$He. Given a Kelvin wave disturbance of wave number $k$ and

amplitude $\eta$, the resulting total linear energy density on the core is given by [9]

$$\frac{E_k}{L} = \frac{\rho\kappa^2}{4\pi} k^2 \eta^2 \left( \ln\left(\frac{1}{ka}\right) + c_1 \right), \tag{1.8}$$

where $c_1 \sim 1$.

## 1.6 Kelvin Wave Heating Model

As mentioned previously, Anand Swaminathan conducted many studies with the goal of trying to understand the mechanisms behind these anomalous free decays. By testing various models and solving for their corresponding theoretical free decay curves, he arrived at the conclusion that none of the models could accurately fit the anomalous free decay data, and that another fitting parameter would be needed; there was a lack of ability in fitting the curve of the bump in the "bulge-like" behavior while simultaneously meeting the kink point of the data. From this it was concluded that connecting the drag force to the critical velocity at which the vortex is depinned is too simple a model to describe the underlying physical processes in the system.

Ultimately, Anand Swaminathan's primary conclusion was that in order to accurately fit the data, there needed to be two critical velocities involved in the theory. His idea was the following: when the third sound flow reaches a critical velocity, $v_{c-cold}$, the Magnus force depins the vortex from a defect in the substrate. The vortex then proceeds to drag along the substrate, dissipating energy. However, this dragging along the substrate is not just a simple static drag dissipating a linearly proportional amount of energy. This dragging is in fact a dynamic process, and the very dragging along the subtrate generates wave disturbances (Kelvin waves) on the vortex core that propagate away from the substrate. This disturbance then travels up the vortex core, reflects at the surface of the thin film, and propagates back down the core. This reflected wave results in an agitation of

the vortex, or heating, that makes it more difficult for the vortex to repin to the substrate. When the third sound flow oscillates back down below the depinning critical velocity, it in fact does not repin until a critical velocity lower than the original depinning one, $v_{c-hot} < v_{c-cold}$, due to this agitation and heating. Eventually, it repins to the substrate at this lower critical velocity, where the vortex agitation created by the dragging dissipates fully in the time between pinning and the beginning of the next cycle of third sound flow, and the process repeats itself. Time scales can be seen to be to be adequate for such relaxation in between cycles by simply considering the group velocity of the slow branch associated with the lowest quarter-wave mode of motion (.1 m/s for a film height of nanometers), and comparing it to the period of third sound oscillations, which is on the order of milliseconds.

Motivated by experimental [6] and theoretical [10] results in the literature, Anand Swaminathan proposed this "Kelvin Wave Heating Model" as a possible explanation for the need for two separate critical velocities. It is the development of a quantitative model of vortex "heating" that can explain the anomalous free decays that we concern ourselves with throughout this thesis.

# Ch.2 Vortex Heating and Depinning

## 2.1 Kelvin Wave Agitation

In Section 1.6, the concept behind the Kelvin Wave Heating Model was detailed. In this section, attempts are made to quantitatively describe vortex agitation that is induced by dynamic interaction with the substrate in order to test whether this agitation could result in a plausible reduction of the cold critical velocity, $v_{c-cold}$, to some lower critical velocity, $v_{c-hot}$. We proceed by considering the reflection coefficient that the change in geometry from vortex core to open surface would create, and use the calculated reflected Kelvin wave amplitude to determine what magnitudes of effective temperatures could be generated on the core by implementing the Planck distribution. Additionally, a model is developed relating the slope change of the vortex core at the defect boundary, resulting from a reflected Kelvin wave, to a reduction in the critical velocity.

Prior to the development of these models, Figure 2.1 is presented as a visual reminder of the qualitative ideas that will be put together in this chapter:

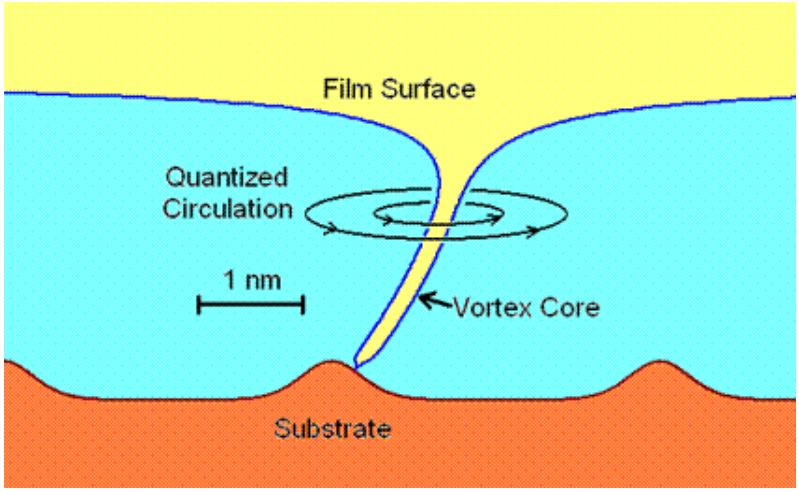


Figure 2.1 - Quantized vortex on a substrate.

In Figure 2.1, one can imagine a quantized vortex dragging along a substrate, generating Kelvin wave disturbances that propagate up the core and out onto the surface of the thin film (the wave modes on the thin-film surface are known as ripplons [3]), with the change in geometry of the vortex core causing a reflection of a portion these disturbances back down the core. It should be noted that an actual quantized vortex does not have the precisely defined shape that is depicted in Figure 2.1. Vortex geometries are determined using classical models, and do not take into account the uncertainty principle. One should therefore imagine the vortex in Figure 2.1 as a quantum fuzz taking that approximate classical shape.

## 2.2 The Reflection Coefficient

In order to develop the models and ideas mentioned in Section 2.1, we must have some concept about the amount of agitation reflected back down the core compared to the amount propagated outwards onto the surface as ripplons. To solve for this reflection coefficient precisely, one must solve the exact hydrodynamic problem which, at present, has eluded us (see Appendix B for more discussion). In an attempt to approximate the reflection coefficient a vortex might exhibit, we decide to neglect the hydrodynamic details and solve for the reflection coefficient

associated with only the change in geometry of the vortex core's surface. The analytical solution to the wave motion on the surface of the thin film is known, and we use 4th-order Runge Kutta numerical integration to integrate down the core and back to the site of the incident wave. In our calcuation we assume a flat surface and cylindrical core with a fixed local gravity $g$. From the solution of the wave motion on the surface, and at the site of the propagation of the disturbance, we deduce reflection and transmission coefficients associated with the change in geometry of the vortex surface. The equations of motion derived, integration strategy, geometrical reflection coefficient deduction, and general conversation regarding the reflection coefficient can be found in Appendix B.

As one would imagine, the geometrical reflection coefficient is going to be primarily dependent on the exact form of the vortex geometry that we choose to perform our calculations on. Intuitively, if the transition from core to surface is very rapid, one could take this to the extreme limit of a traveling wave incident against a classical wall, and would expect a very large reflection coefficient. Constrastingly, if the geometry of the vortex is such that the expansion occurs gradually from very near to the pinning site, then the change in geometry is much less sudden, and one would predict a negligible reflection coefficient.

Fortunately, the issue of vortex geometry is a topic that has already been dealt with in the history of the Quantum Fluids Laboratory. In 1992, laboratory member Oliver Ryan derived, in his senior thesis [11], the energy and geometry of a superfluid film vortex. This derivation included the effects of kinetic energy due to the rotating fluid, potential energy due to Van Der Waals interactions with the substrate, and surface energy terms. The resulting vortex (Figure 2.2) consists of a very rapid change in geometry, which, intuitively, we expect to result in a significant geometrical reflection coefficient.

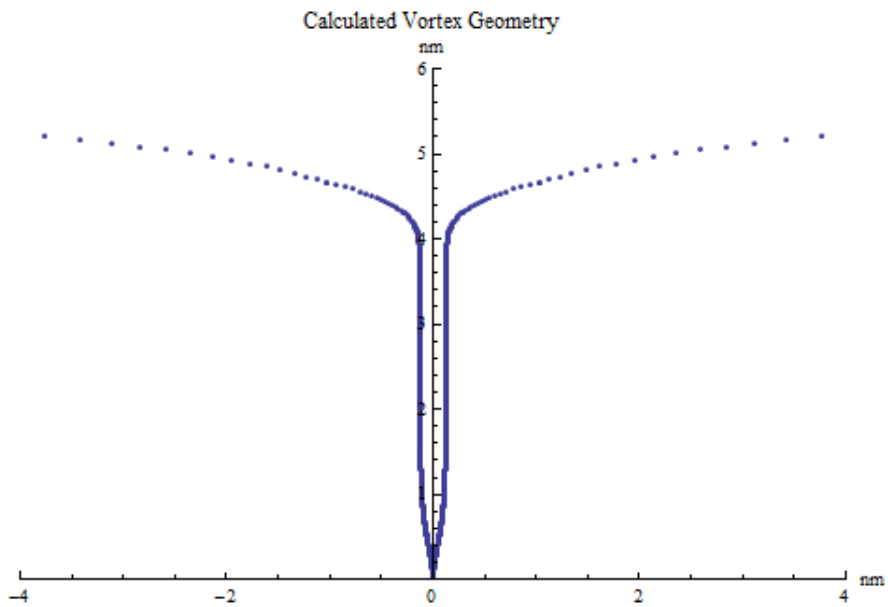


Figure 2.2 - Thin-film vortex geometry as calculated by Oliver Ryan. Note: scale is in nanometers.

When the procedure described in Appendix B is performed using Oliver Ryan's geometry, one calculates a reasonably large reflection coefficient of R = 53% for the lowest frequency, quarter-wave, mode of the system (See Figure 2.6). This is a significant reflection coefficient, implying that a large amount of the propagated energy will be reflected back down the core and result in core heating. However, one cannot take this reflection coefficient too seriously, as it completely ignores the hydrodynamic details of the system. Yet another failure of the model is that it assumes a constant local gravity on the core length, which clearly cannot be true. Work was done to try to incorporate a position dependent local gravity into the simulation, but was ultimately met with failure.

Since we cannot solve the exact hydrodynamic problem, we are unable to determine the exact reflection coefficient, and cannot make any strong conclusions regarding the precise amount of agitation retained on the core. However, the rather rapid change in the geometry calculated in Oliver Ryan's thesis suggests that the reflection coefficient should indeed be non-negligible, due to geometrical

considerations alone. If a solution to the mathematical problem of the reflection coefficient could be found, it would be a great step in speaking quantitatively about the retained agitation in the system. However, much important information can still be gleaned by using an arbitrary reflection coefficient, R, as a parameter, and continuing with the development of the Kelvin Wave Heating Model that was proposed. This is precisely what will be done in the following sections.

## 2.3 Effective Planck Temperature

Previous work has been done in the Quantum Fluids Laboratory studying the temperature dependence of dissipation in third sound free decays [12]. Studies were performed where the theory of third sound dissipation involved an Arhennius-type barrier to the thermally activated depinning of quantized vortices on the substrate. In these studies, previous researchers were able to correlate the likelihood of a vortex depinning to the strength of the background flow, as well as an effective temperature of the vortex away from thermal equilibrium, which was built into a Boltzmann factor. These studies concluded that, by implementing this model, an effective vortex temperature of .95 K was associated with a vortex's depinning.

In the Kelvin Wave Heating Model, Kelvin waves are propagated up the core due to the interaction of the vortex with the substrate. One could conceivably link the amplitudes of these generated Kelvin waves to a thermally induced root-mean-squared deviation from the core equilibrium by comparison to the Planck distribution, resulting in an effective temperature of the vortex away from equilibrium. In the rest of this section, we develop a model for vortex tip interaction with the substrate, determine the amplitudes of Kelvin waves generated on the vortex core resulting from this model, and calculate the effective Planck distribution temperature associated with these Kelvin wave amplitudes with the hope of generating temperatures on the order of 1 K that have been found in previous studies.

We begin with a very simple model for the motion of the vortex tip in order to provide a general idea of what kinds of magnitudes of disturbances are being propagated up the core by interaction with the substrate. Our model is the following: Assume a vortex is pinned to a defect site. The third sound flow then increases to the point that the Magnus force depins the vortex core at a yet to be determined cold critical velocity. The vortex tip then proceeds to move across the substrate at the speed of the background flow, $v_s$, where after a time, $\tau$, the third sound flow decreases below the cold critical velocity, and the vortex abruptly repins to the next defect on the substrate, a distance $\lambda$ away from the previous pinning site. If the reader is concerned that this model does not explicitly incorporate a $v_{c-hot}$, this issue will be addressed in Section 2.4. See Figure 2.3 below for a graphical representation of this model.

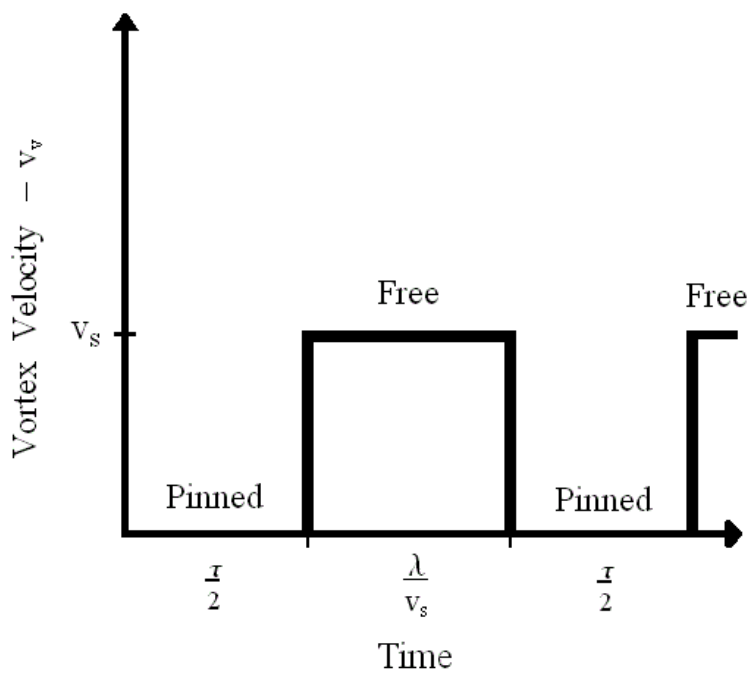


Figure 2.3 - Velocity versus time plot of the motion of the vortex tip.

We describe this model mathematically by Equation 2.1

$$v(t) = \begin{cases} 0 & 0<t<\frac{\tau}{2} \ and \ \frac{\lambda}{v_v}-\frac{\tau}{2}<t<\frac{\lambda}{v_v} \\ v_s & \frac{\tau}{2}<t<\frac{\lambda}{v_v}-\frac{\tau}{2} \end{cases}, \tag{2.1}$$

where Equation 2.2, below, is the condition required for the model to be self-consistent (requiring that the vortex moves at an average speed of $v_v$ over the whole time interval $\tau + \frac{\lambda}{v_s}$).

$$\tau = \lambda(\frac{1}{v_v} - \frac{1}{v_s}) \tag{2.2}$$

We proceed by Fourier analyzing the vortex tip motion and determining the Fourier coefficients associated with its designated velocity conditions. Performing a Fourier decomposition of Equation 2.1 results in coefficients of

$$a_n^{v(t)} = \frac{2v_s}{n\pi} sin(\frac{v_v n\pi\tau}{\lambda}) \text{ ; n = 1, 2, 3, ...} \tag{2.3}$$

corresponding to a reconstruction of $v(t)$ in terms of an infinite sum of cosine functions

$$v(t) = \sum_{n=1}^{\infty} a_n cos(\frac{v_v n\pi t}{\lambda}) \tag{2.4}$$

that can be integrated with respect to time to yield the corresponding position reconstruction of the motion of the tip relative to the mean vortex position

$$x(t) = \sum_{n=1}^{\infty} \frac{\lambda}{2v_v n\pi} a_n sin(\frac{2v_v n\pi t}{\lambda}) \tag{2.5}$$

Combining Equations 2.3 & 2.5, and rewriting the maximum amplitude of the *nth* Fourier mode results in the expression

$$\eta_n = \frac{\lambda}{2v_v n^2 \pi^2} v_s sin(\frac{v_v n \pi \tau}{\lambda}) \tag{2.6}$$

Equation 2.6 allows one to calculate an amplitude of wave motion, $\eta_n$, propagated up the core associated with our model for vortex motion depending on the critical velocity, $v_c$, vortex velocity, $v_v$, and distance between pinning sites, $\lambda$. At present, our model generates wave disturbances of a particular amplitude, $\eta_n$, that will propagate up the core from the resonator surface. Based on our previous discussion, and the literature [10], we have reason to believe that these disturbances will be Kelvin waves and will obey the dispersion relation of Equation 1.6. Additionally, it is useful to note that associated with this Fourier amplitude of wave motion pumped up the core, $\eta_n$, there is a Fourier frequency (or Kelvin wave frequency), $\omega_{pumped}$, given by:

$$\omega_{pumped} = \frac{2v_v n \pi}{\lambda} \tag{2.7}$$

It should quickly be mentioned that in our system it is desirable to have a means of coupling the Kelvin waves on the vortex core with the ripplons on the surface of the thin-film. Therefore, we have rederived Equations 1.6 and 1.8[1] to include a surface tension term $\gamma$ , which for superfluid $^4$He is $3.54 \times 10^{-4} \frac{N}{m}$, that allows us to more coherently couple the wave motion on the core with the wave motion on the surface of the thin film:

$$\omega^{\pm}(k) = \frac{\kappa}{2\pi a}\left(-1 \mp \sqrt{\left(1 + \frac{(ka)K_0(ka)}{K_1(ka)}\right)(1 + \Gamma(ka)^2)}\right) \tag{2.8}$$

and

$$\frac{E_k}{L} = \frac{\rho\kappa^2}{4\pi} k^2 \eta^2 \left(\ln\left(\frac{2}{ka}\right) - \gamma - \frac{1}{2}\right) \tag{2.9}$$

[1]Private Communication F. Ellis

where $\Gamma = (2\pi)^2 \frac{\gamma a}{\rho \kappa^2}$.

Using the dispersion relation for the slow branch of a Kelvin wave (Equation 2.8), $\omega_{pumped}$ can be converted into a Kelvin wavenumber $k_{pumped}$. We can then use Equation 2.9 to calculate the energy associated with a given Kelvin wave disturbance, $\eta$, and wavenumber, $k$. This provides us with a value for the amount of energy pumped up the core, $E_{pumped}$ , by a Kelvin wave associated with a disturbance propagating upward from the substrate due to our vortex tip motion model.

Next, we invoke our reflection coefficient parameter and state that some fraction of the energy pumped up the core, $R$, is going to be reflected back from the change in geometry of the vortex core surface:

$$E_{Reflected} = R \times E_{pumped} \tag{2.10}$$

and use $E_{Reflected}$ and Equation 2.9 (under the assumption that the wavenumber does not change upon reflection) to reversely calculate a reflected amplitude of the Kelvin wave, $\eta_{Reflected}$.

We have now determined the reflected wave amplitude associated with our velocity model and reflection coefficient. We wish to turn this into a thermal rms amplitude deviation associated with some effective temperature of the vortex core, $T$. We use the standard form of the Planck Distribution, $n_q$ [13], and define the rms amplitude fluctuation as:

$$< \eta^2 >_q = \eta_q^2 n_q = \frac{\eta_q^2}{e^{\frac{\hbar\omega_q}{k_B T}} - 1} \tag{2.11}$$

where $\eta_q^2$ can be found by rearranging Equation 2.9, $E_q = \hbar\omega_q$, and $k_B$ is Boltzmann's constant (Note: the notation of wavenumber has changed from $k \rightarrow q$ to avoid confusion with Kelvin and Boltzmann notation).

Using the scaling $\tau_k = 2\pi a^2 k_B T/\hbar\kappa$, $x = qa$, and letting $L = h_0$, where we say the vortex extends the height of the thin-film, $h_0$, Equation 2.11 can be rewritten using the integral approximation:

$$\sqrt{<\eta^2>_x} = \sqrt{\frac{2\hbar}{\rho\kappa h_0}}\left(\frac{1}{x\sqrt{ln(\frac{2}{x})-\gamma-\frac{1}{2}}}\right)\sqrt{\frac{\sqrt{\left(1+\frac{xK_0(x)}{K_1(x)}\right)(1+\Gamma x^2)}-1}{e^{\frac{\sqrt{\left(1+\frac{xK_0(x)}{K_1(x)}\right)(1+\Gamma x^2)}-1}{\tau_k}}-1}} \tag{2.12}$$

One can then find the roots of Equation 2.12 to determine the value of the scaled effective temperatute, $\tau_k$, associated with $\eta_{Reflected}$. Using the parameters of our model (distance between pinning sites, critical velocity, and reflection coefficient), we can estimate the effective Planck distribution temperatures generated by our vortex moving from one pinning site to another. A sampling of results are provided in Figure 2.4 and Figure 2.5.

We find that the reflection coefficient results in having an effect on the generated effective temperature approximately linearly associated with its magnitude (a reduction of the reflection coefficient by 20% results in a reduction of the effective temperature, $T$, by approximately 20%). One also discovers an increase in the effective temperature, $T$, associated with an increase in the distance between defect sites, $\lambda$. This result is due to the fact that the farther the vortex travels between pinning sites, the more weight will be give to the lowest mode of the Fourier decomposition, and consequently larger amplitudes of Kelvin waves will result from larger distances between defect sites.

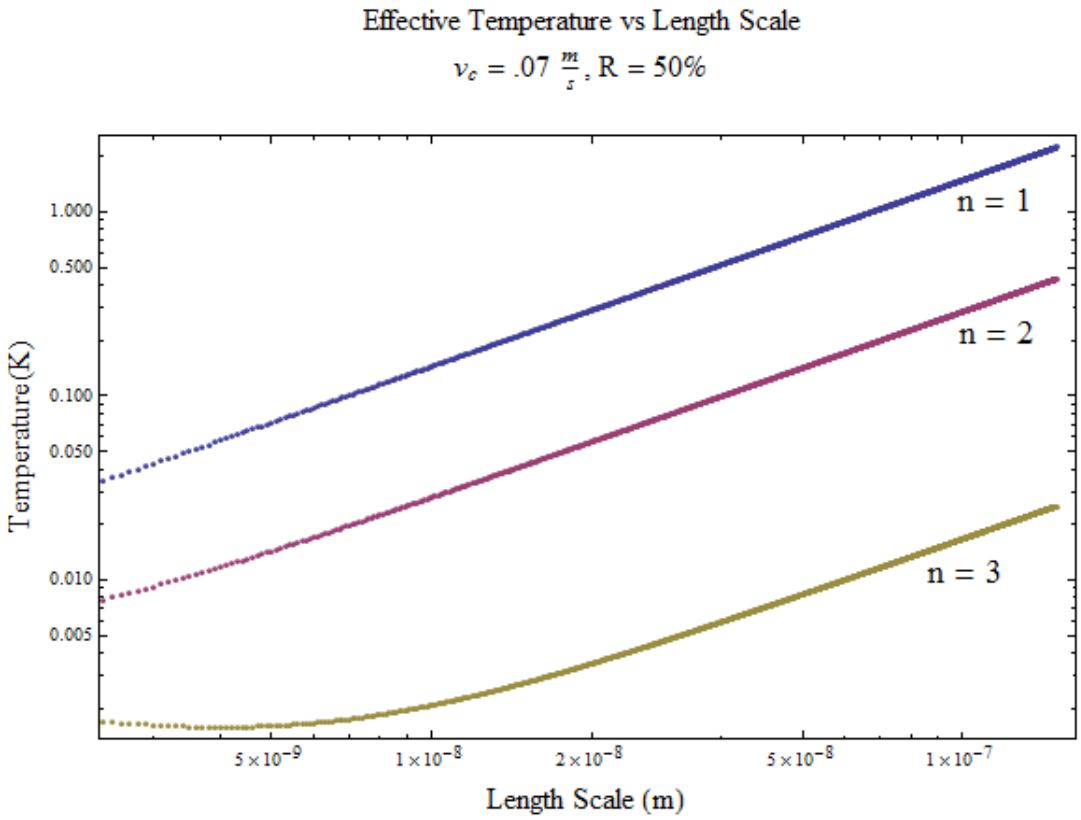


Figure 2.4 - Effective Temperature vs Length Scale ($\lambda$) plots with a reflection coefficient of 50%.

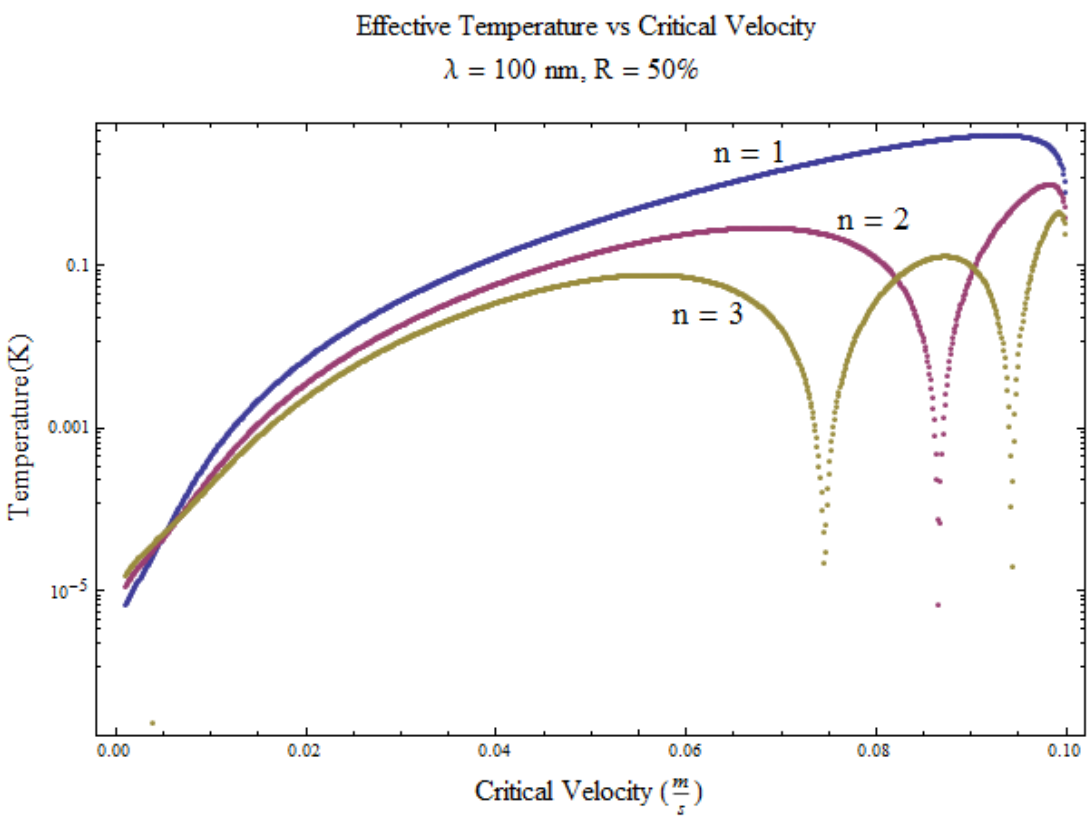


Figure 2.5 - Effective Temperature vs Critical Velocity plots with a reflection coefficient of 50%. Note: the discontinuities and decreasing values of the temperature in the Fourier modes are merely a result of resonance in the Fourier analysis, and do not represent physical phenomena.

While not quantitatively rigorous, when one selects values of the model's parameters derived from physical expectations ($v_c = .01 - .1\frac{m}{s}$, $\lambda = 1$ nm - 100 nm), this model is capable of generating Boltzmann temperatures in line with what was witnessed in previous Quantum Fluids Laboratory experiments. However, one must understand that the critical velocity is really the only parameter that can be narrowed down into any confident range, as determined by previous Quantum Fluids Laboratory experiments. The length scale parameter is undoubtedly highly variable, and unknown without experimental analysis from a technique like scanning electron microscopy. Similarly, we do not know enough about the value of the reflection coefficient, due to the neglect of the hydrodynamic details, to

place it in any reasonable range. Regardless, by approximating many of these physical parameters, we can see that perhaps the Kelvin Wave Heating Model is capable of providing some insight into the mechanism of these previously studied thermal barriers to depinning. While this model is not as rigorous as one would like, it does suggest that dynamic vortex interaction with the substrate could be an important phenomenon in these experimental systems. Deriving a more rigorous model for vortex interaction with the substrate (perhaps using the model that will be developed in Chapter 4), and applying it in order to get a more definitive determination of the effective Planck distribution temperature that could be compared with .95 K, could prove to be an interesting project for a future Quantum Fluids Laboratory student.

## 2.4 Reduction of the Critical Velocity

Before moving on from this model of dynamic vortex interaction with the substrate to something more sophisticated, it will be informative to see how one can use this model to induce a reduction in the critical velocity, as well as to generate the actual vortex dynamics resulting from Kelvin wave heating. From the Schwarz paper [5], it is known that every quantized vortex must obey a boundary condition such that the vortex intersects a surface orthogonally. If one considers a simple spherical pinning defect on the substrate (Figure 2.6), then one can see that if there is Kelvin wave agitation on the vortex core, there is only so much leeway that a vortex has to deal with a geometrical distortion before it is necessarily required by its boundary condition to detach from the defect site.

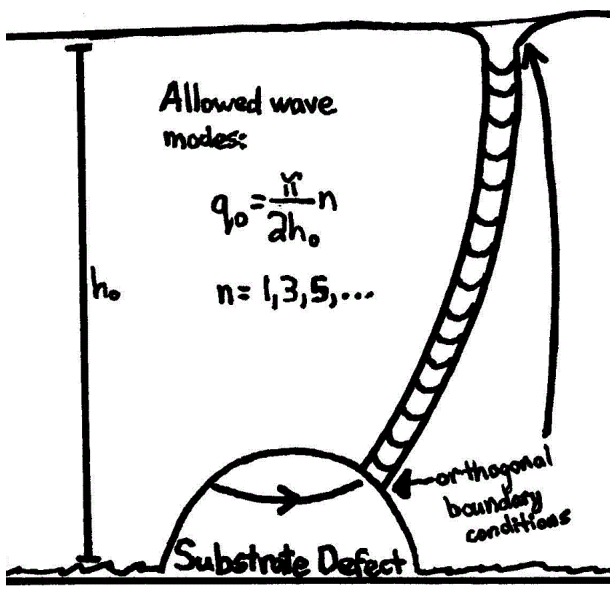


Figure 2.6 - A vortex pinned to a defect site trying to meet its boundary condition. Note: not drawn to scale.

If one narrows one's view down to the defect site and uses Newton's Second Law to balance the Magnus force (pinning force at the critical velocity) on the

vortex with the parallel component of the vortex line tension, one can determine the slope of a vortex (with no wave agitation) locally around the defect site to be

$$s_0 = \frac{4\pi h v_{c-cold}}{\kappa Log[\frac{b}{a}]} \tag{2.13}$$

where $a$ is the radius of the vortex core, and $b$ is the radial extent of a vortex's circulation. Observing the vortex very locally like this is a crude model, but it provides us with a fast and simple means of estimating what we are seeking. A more sophisticated model will be developed in Chapter 3.

Now that we have a value for the unperturbed slope, we take our $\eta_{Reflected}$ disturbance, and associate with its amplitude and wavenumber a change in the slope of the vortex:

$$\triangle s = q_{pumped}\eta_{Reflected} \tag{2.14}$$

We assume that given some Kelvin wave agitation, the vortex will be less likely to pin, i.e. the critical velocity will be decreased. Therefore, as a rough model, we associate with our disturbance, $\triangle s$, a simple linear reduction in the critical velocity given by:

$$v_{c-hot} = (1 - \frac{\triangle s}{s_0})v_{c-cold} \tag{2.15}$$

Equation 2.15 says that given some disturbance, our original critical velocity will be reduced by an amount linearly proportional to the disturbance on the vortex core related to how "difficult" it is now for the vortex core to meet its orthogonal boundary condition with the substrate. $s_0$ is the value of the unperturbed equilibrium slope of the vortex near the pinning site, and is thus implemented as a characteristic value for slope magnitudes in this system that serves as a reference point for the slope change in Equation 2.15. There is no physical basis for

choosing a linear reduction; it is merely the simplest possible form that will result in a reduced critical velocity.

## 2.5 Self-Consistent Dynamics

Since we now have a means of expressing the reduction of the critical velocity, it will be interesting to calculate the resulting modified vortex dynamics. We are particularly interested in the relationships among $v_s$, $v_v$, and $v_c$, and require the magnitude of the velocity of our vortex given by Equation 1.5. Therefore, we use the Pythagorean theorem to modify Equation 1.5 to deal with only the magnitude of the vortex velocity:

$$| v_v |= \sqrt{v_s^2 - v_c^2} \tag{2.16}$$

Using Equations 2.13, 2.14, & 2.15, and solving self-consistently with Equation 2.16, one cannot derive an analytic expression relating $v_s$, $v_v$, and $v_c$. Therefore, we approach the problem in a numerical fashion to determine these relations. We assume an oscillatory third sound flow of the background superfluid, $v_s$. We then guess a value of the vortex velocity, $v_v$, and calculate the critical velocity using Equation 2.16, calling that value $v_{c-initial}$. Then we use the model described in Section 2.3 to determine an $\eta_{Reflected}$ (using our guess for $v_v$), and utilize Equations 2.14 & 2.15 to reduce the critical velocity by some change in the slope due to the Kelvin wave disturbance, $\eta_{Reflected}$, resulting in a calculated critical velocity, $v_{c-final}$. Finally, we compare our initial and final critical velocities. If they differ by more than a given tolerance, $\delta_{convergence}$, then we guess a different starting $v_v$ and repeat the procedure until our convergence condition is met:

$$| v_{c-initial} - v_{c-final} |< \delta_{convergence} \tag{2.17}$$

This procedure must be performed for all values of the superfluid flow, $v_s$, in order to develop a total picture of the vortex dynamics at all the values of the superfluid velocity in a third sound oscillation. The results of these simulations are provided in Figures 2.7 & 2.8.

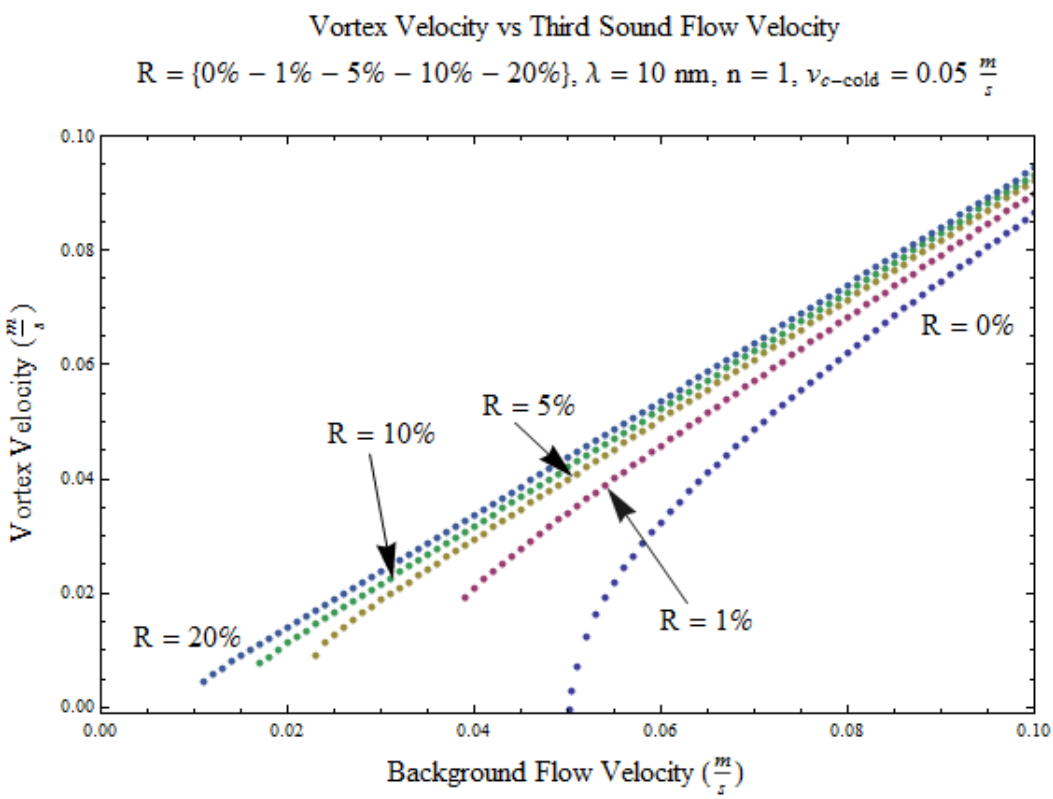


Figure 2.7 - Plot of vortex velocity ($v_v$) vs third sound flow velocity ($v_s$) for different values of the reflection coefficient.

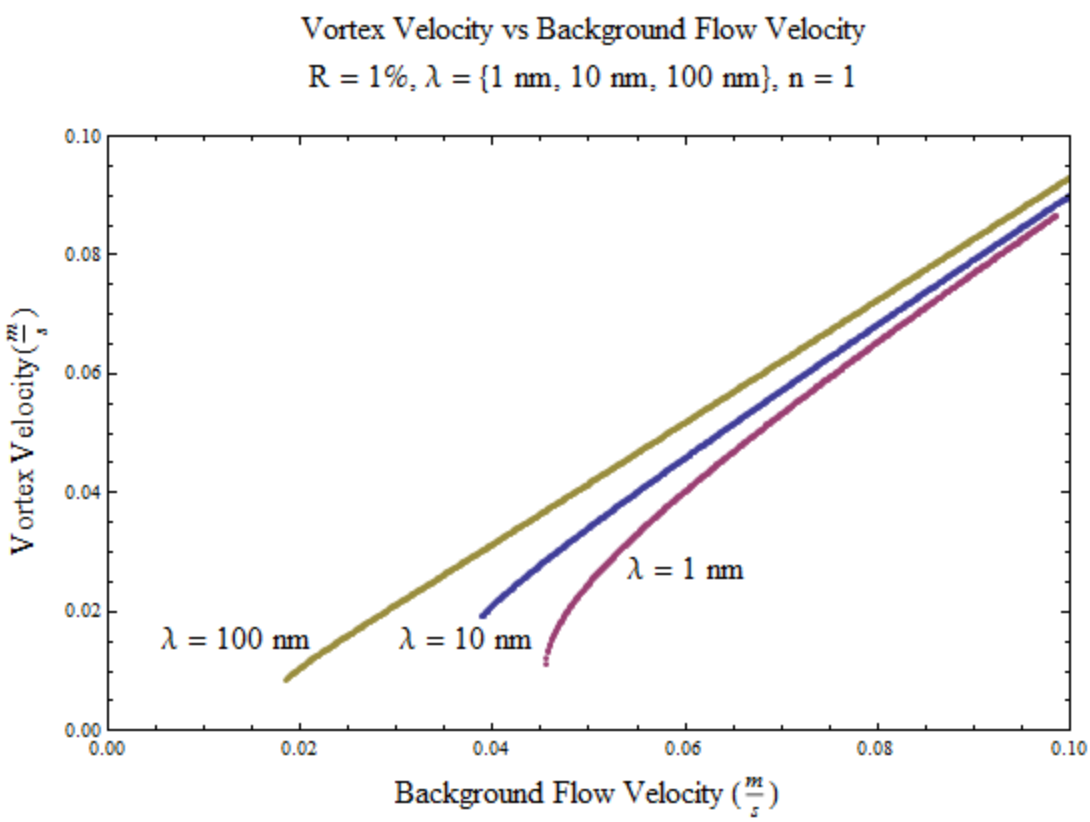


Figure 2.8 - Plot of vortex velocity ($v_v$) vs third sound flow velocity ($v_s$) for different values of the length scale $\lambda$.

Figure 2.7 and 2.8 clearly show a reduction in the critical velocity when compared to the static drag dynamics ($R = 0\%$ - the blue curve in Figure 2.7). In the case of a reflection coefficient of 0%, all of the agitation is transmitted out of the vortex core, no heating occurs, and the solution is simply that which is expected from Equation 2.16. If the reflection coefficient, or length scale, is increased in value, we see that the steady state solutions to the vortex motion result in a repinning at a much lower critical velocity than when it was depinned, i.e. the lowest value of $v_s$ in Figures 2.7 & 2.8 at which a solutions still exists, for a given curve. It is important to note again that these are the steady state solutions to the vortex motion (which is the condition of Equations 1.5 & 2.16). In Figures 2.7 and 2.8, the simulations run with nonzero reflection coefficients have no solution for some values of the superfluid flow velocity. Clearly, a vortex cannot have

a nonzero velocity and suddenly repin to the bump and be motionless, with no intermediate deceleration. Since these solutions are derived in the steady state, a physical interpretation of this region where no solution exists would be that this region is a point of hysteresis where the vortex is captured by the defect site and exhibits hysteretic motion as it settles down into a pinned state. This process is depicted in Figure 2.9, which is a very important figure for understanding the vortex dynamics being discussed.

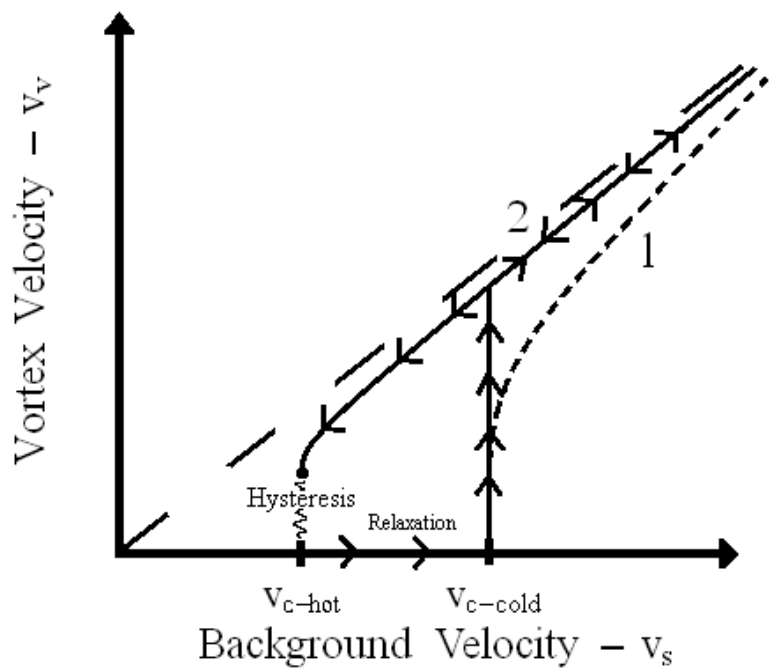


Figure 2.9 - Modified vortex dynamics. The vortex depins at $v_{c-cold}$, transfers to path 2, travels up path 2 to the peak of the third sound oscillation, then travels back down path 2, where it undergoes hysteretic motion when captured by the defect site at $v_{c-hot}$, and eventually repins. Paths 1 and 2 represent the static and dynamic drag paths, respectively.

## 2.6 Summary

In this chapter we have developed a rudimentary model for Kelvin wave heating based on a vortex moving from one pinning site to another along the surface of a substrate. Ultimately, this model fails at being a quantitative guide to Kelvin wave heating due to the fact that we cannot pin down the reflection coefficient of the vortex, or the length scale between defect sites, with any reliable accuracy. However, we do learn that given values of the reflection coefficient and the length scale that one might reasonably guess in our experimental system, meaningful effective temperatures can be generated that corroborate results found in previous studies. Additionally, from our slope argument, we learn that significant reductions in the critical velocity can occur due to Kelvin wave heating and, while not rigorous, this model serves as strong motivation for developing a more complete theory. Lastly, it is to be noted that thinking in terms of the frequency properties of the substrate has been instructive in this chapter and is an important technique that will be adopted as a strategy throughout the remaining chapters.

# Ch.3 Substrate Analysis

## 3.1 Motivation

Most information, to date, regarding the critical velocity has been derived from experimental results. Theoretically, it has been generally believed that a defect site (geometrical distortion) on a perfectly flat substrate provides an energy minimum which the vortex falls into, resulting in the vortex pinning to the defect. It would be useful to be able to relate the pinning force that acts on a vortex to the geometrical properties of an arbitrary surface. This would allow one to relate experimental critical velocities to the surface properties of the substrate, and would give one some idea of the characteristics of the resonator substrate that we are unable to measure directly. Likewise, if the exact geometry of a resonator substrate could be specified, then one could exactly calculate the pinning force at all points on the resonator surface.

When a vortex moves across an arbitrary surface in one dimension, the vortex will exert a suctioning force on the surface it is moving across (think of a tornado traveling over a cornfield, ripping corn out of the ground around its core as it moves along its path). In a macroscopic, classical vortex scenario, this suction is caused by Bernoulli pressure differences that result from the velocity field of the vortex interacting with the surrounding surface geometry. We choose to model our quantized vortex classically to determine the suction force on the substrate resulting from this Bernoulli pressure field. We then claim that a vortex, having zero mass, can have no net forces acting on it. Therefore, the component of the suction force parallel to the substrate must be equal to the pinning force when the vortex is immobilized on a defect site, and we should be able to correlate the

geometrical properties of our surface to the pinning force (critical velocity) that a vortex experiences on the substrate.

## 3.2 Surface Geometry

In getting started, it is helpful to understand the normal vector geometry of an arbitrary surface, i.e. to come up with relations for the normal vectors of an arbitrary two-dimensional surface, $\eta(x, y)$ (Figure 3.1).

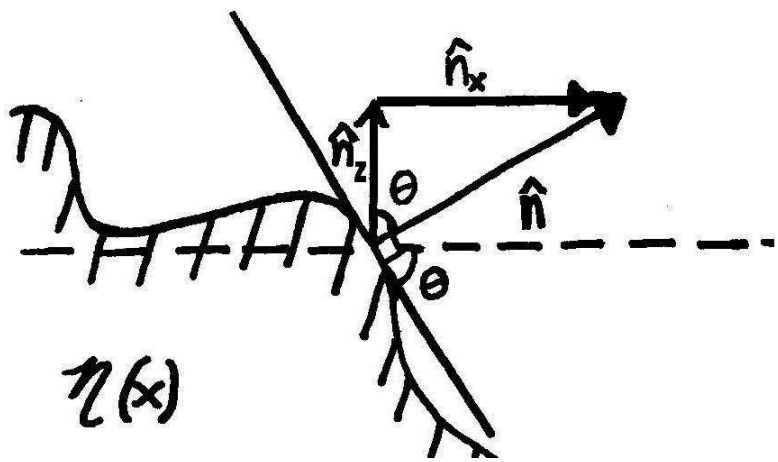


Figure 3.1 - A two-dimensional slice of the normal vectors for an arbitrary three-dimensional surface $\eta(x, y)$.

From Figure 3.1 we can deduce a relationship among the normal vectors:

$$\frac{\hat{n}_z}{\hat{n}_x} = \frac{1}{-\frac{\partial \eta}{\partial x}} \text{ or } \frac{\hat{n}_x}{\hat{n}_z} = -\frac{\partial \eta}{\partial x} \tag{3.1}$$

We additionally require that the "normal" vectors be normalized to unity:

$$\hat{n}_x^2 + \hat{n}_z^2 = 1 \tag{3.2}$$

Combining Equations 3.1 & 3.2, along with the Pythagorean theorem, one can deduce Equation 3.3.

$$\hat{n}_x = \frac{-\frac{\partial \eta}{\partial x}}{\sqrt{1+\left(\frac{\partial \eta}{\partial x}\right)^2}} \tag{3.3}$$

Similarly, in a three-dimensional analysis, one can follow this methodology to derive the more general Equation 3.4, where $\hat{\imath}$ and $\hat{\jmath}$ refer to two orthogonal units vectors that are parallel to the substrate surface:

$$\hat{\imath} n_x + \hat{\jmath} n_y = -\frac{\vec{\nabla}\eta(x,y)}{\sqrt{1+\left|\vec{\nabla}\eta(x,y)\right|^2}} \tag{3.4}$$

In addition to the normal vector geometry, we will need to understand the relationship between the area of an arbitrary surface, $dA$, compared with the perpendicular area actually exposed to the velocity field of the vortex core, $dA_\perp$. The relationships between these two areas is illustrated in Figure 3.2

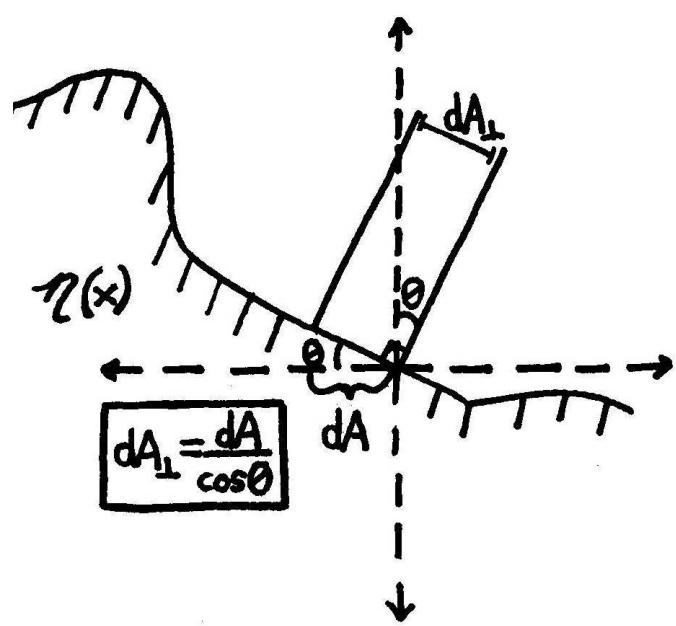


Figure 3.2 - Differential area analysis of an arbitrary surface.

## 3.3 Bernoulli Pressure Integration

We seek to find, given an arbitrary surface, the total Bernoulli force exerted parallel to the substrate at $\overrightarrow{r}$ due to a straight vortex core at $\overrightarrow{r_v}$. We assume a straight vortex core, as it greatly simplifies the mathematics involved. Dealing with the velocity field generated by a distorted vortex core would be a very mathematically demanding scenario, and we just seek a rough estimation of the pinning force. In order to do this, we must integrate $d\overrightarrow{F_x}$ (change of notation $d\overrightarrow{F_x} \rightarrow d\overrightarrow{F_\parallel}$, the force parallel to the substrate), in order to get the total force exerted parallel to the substrate, where

$$d\overrightarrow{F_\parallel} = PdA\hat{n} \cdot \hat{i} = -\frac{1}{2}\rho\frac{\hbar^2}{m_4^2}\frac{1}{(\overrightarrow{r}-\overrightarrow{r_v})^2}dA_\perp\hat{n} \cdot \hat{i} \tag{3.5}$$

Integrating Equation 3.5 we arrive at:

$$\overrightarrow{F_\parallel} = \iint -\frac{1}{2}\rho\frac{\hbar^2}{m_4^2}\overrightarrow{\nabla}\eta(x,y)\frac{1}{(\overrightarrow{x}-\overrightarrow{x_v})^2+(\overrightarrow{y}-\overrightarrow{y_v})^2}dxdy \tag{3.6}$$

We attack this integration via a Fourier convolution of the terms $\overrightarrow{\nabla}\eta(x,y)$ and $\frac{1}{(\overrightarrow{x}-\overrightarrow{x_v})^2+(\overrightarrow{y}-\overrightarrow{y_v})^2}$, and we begin by defining a forward and backward Fourier transformation of the substrate, $\eta(x,y)$:

$$\tilde{\eta}(q) = \frac{1}{2\pi}\iint_{-\infty}^{\infty}\eta(x,y)e^{-i\overrightarrow{q}\cdot\overrightarrow{r}}d^2r \textbf{ and } \eta(x,y) = \frac{1}{2\pi}\iint_{-\infty}^{\infty}\tilde{\eta}(\overrightarrow{q})e^{i\overrightarrow{q}\cdot\overrightarrow{r}}d^2q \tag{3.7}$$

It is useful at this point to mention that in performing this analysis the solution will ultimately be intimately linked to the frequency properties of the Fourier transformation of our arbitrary substrate. Thinking in terms of the frequency and wavenumber components of our system was not only useful in Chapter 2, as well as this chapter, but will also be key in the more sophisticated treatment of the

critical velocity reduction model that will occur in Chapter 4. We continue with our analysis by taking the gradient of the backward transformation (Equation 3.7):

$$\vec{\nabla}\eta(x,y) = \frac{i}{2\pi}\iint_{-\infty}^{\infty} \vec{q}\,\tilde{\eta}(q)e^{i\vec{q}\cdot\vec{r}}d^2q \tag{3.8}$$

We can clean up Equation 3.8 for conceptual purposes by defining:

$$\vec{\tilde{G}}(\vec{q}) = \frac{i}{2\pi}\vec{q}\,\tilde{\eta}(\vec{q}) \tag{3.9}$$

and rewriting Equation 3.9 as:

$$\vec{\nabla}\eta(x,y) = \iint_{-\infty}^{\infty} \vec{\tilde{G}}(\vec{q})e^{i\vec{q}\cdot\vec{r}}d^2q \tag{3.10}$$

Regarding the $\frac{1}{r}$ inverse flow field term, one can see that at some point in this analysis we are going to run into some troublesome behavior as $\vec{r} \to \vec{r_v}$. This is expected, as in Chapter 1 we discussed how a vortex is defined as possessing a $\frac{1}{r}$ flow field up until the core radius, where quantitatively different behavior occurs as $r$ becomes less than $a_0$ . This is the same issue that we run into at present.

Since we are trying to define a Fourier transform of the inverse flow field term, it is necessary that we integrate through the singularity somehow without causing any unwieldy infinities. There are a couple of conceivable ways of doing this, but we choose the path that allows for the cleanest analytical solution to this integral. We introduce a "damping" term, $\gamma_d$, in the denominator of the inverse flow field part of the convolution, which is approximately equal to the core radius, $a_0$ (Equation 3.11).

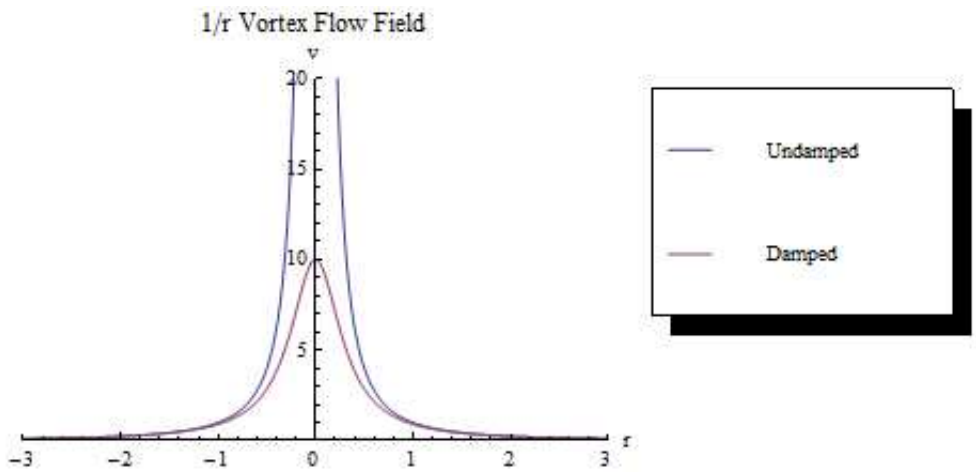


Figure 3.3 - The utility of the damping term in controlling the singularity of the velocity field.

By introducing this damping term, we can write the Fourier transform of the inverse flow field part of the convolution in polar coordinates, and simplify it down to the expression

$$\tilde{p}(\overrightarrow{q'}) = \frac{1}{2\pi} e^{i\overrightarrow{q'}\cdot\overrightarrow{r_v}} \iint \frac{e^{-i\overrightarrow{q'}\overrightarrow{r}Cos[\phi]}}{r^2+\gamma_d^2} r d\phi dr = e^{iq'\overrightarrow{r_v}} K_0(q'\gamma_d) \ , \tag{3.11}$$

where $K_0$ is a modified Bessel function of order zero. For future ease, let us also define the Fourier transform of the pressure field:

$$\tilde{p}(\overrightarrow{q'}) = e^{i\overrightarrow{q'}\overrightarrow{r_v}} \tilde{p}_0(\overrightarrow{q}') \tag{3.12}$$

where

$$p(\overrightarrow{r}) = \iint_{-\infty}^{\infty} \tilde{p}(\overrightarrow{q'}) e^{i\overrightarrow{q'}\cdot\overrightarrow{r}} d^2q' \tag{3.13}$$

Now, one can write out the full convolution expression:

$$\overrightarrow{F_{\parallel}} = -\frac{1}{4\pi}\rho\frac{\hbar^2}{m_4^2}\iint_{x,y}\left[\iint_{q}\overrightarrow{\tilde{G}}(\overrightarrow{q})e^{i\overrightarrow{q}\cdot\overrightarrow{r}}d^2q\iint_{q'}\tilde{p}(\overrightarrow{q'})e^{iq'\cdot\overrightarrow{r}}d^2q'\right]dxdy \tag{3.14}$$

After performing the proper algebra and integrations, Equation 3.14 can be reduced into the form:

$$\overrightarrow{F_{\parallel}}(r_v) = -\frac{i}{2}\rho\frac{\hbar^2}{m_4^2}\iint_{q}\overrightarrow{q}\tilde{\eta}(\overrightarrow{q})\tilde{p}(-\overrightarrow{q})d^2q \tag{3.15}$$

In evaluating Equation 3.15, we assume a simple one dimensional uniform translation of the vortex, $\overrightarrow{r_v} = \hat{i}v_vt$, and want to look at the frequency spectrum of the force parallel to the substrate:

$$\overrightarrow{F_{\parallel}}(\omega) = \frac{1}{\sqrt{2\pi}}\int\overrightarrow{F_{\parallel}}(\hat{i}v_vt)e^{i\omega t}dt = -\frac{i}{2\sqrt{2\pi}}\rho\frac{\hbar^2}{m_4^2}\iint\overrightarrow{q}\tilde{\eta}(\overrightarrow{q})\tilde{p}(-\overrightarrow{q})\int e^{i\overrightarrow{q_x}\overrightarrow{v_v}t}e^{i\omega t}dtd^2q \tag{3.16}$$

Equation 3.16 allows one to calculate the force exerted on a vortex parallel to the substrate, or, in equivalent language, the pinning force associated with a vortex moving in one dimension over an arbitrary surface. We seek an intuitive physical understanding of the relationship between the parameters presented. In order to put this equation into the simplest possible form, we choose a one-dimensional surface with only one wavenumber present, i.e. a complex exponential function:

$$\eta(x) = \eta_0 e^{iq_0x} \tag{3.17}$$

Choosing this form of the substrate surface results in an rms force of:

$$|F_{\mathbf{0}}| = \frac{1}{2(2\pi)^{3/2}}\rho\frac{\hbar^2}{m_4^2}q_0\eta_0 K_0(q_0\gamma_d) \tag{3.18}$$

A common result in thin-film superfluid studies is the relation between velocity and force of

$$F = v\rho\kappa h_0 \tag{3.19}$$

which allows us to write our final result relating the critical velocity to the horizontal pinning force between a superfluid vortex and a one-dimensional substrate possessing a single wavenumber, $q_0$, with bumps of a height $\eta_0$:

$$v_{c-cold} = \frac{1}{2(2\pi)^{3/2}}\frac{\hbar^2}{\kappa m_4^2 h_0}q_0\eta_0 K_0(q_0\gamma_d) \tag{3.20}$$

This relation is significant because we now have an analytical means of relating the arbitrary properties of a substrate to the cold critical velocity of a vortex via the interaction of the Bernoulli pressure field of the vortex with the local resonator surface geometry. Figure 3.4 provides a plot of Equation 3.20 using parameters that we might expect to be associated with a resonator substrate. Note that $\eta_0$ should be noticeably smaller than the film height $h_0$ in order to maintain a flat adsorbed thin-film surface.

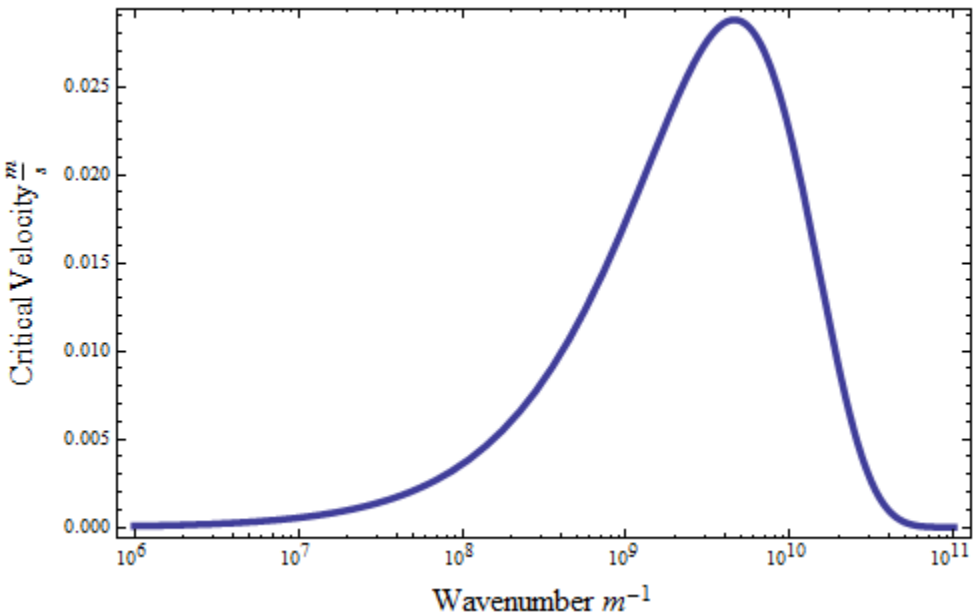


Figure 3.4 - Critical Velocity vs Fourier Wavenumber. A plot of Equation 3.20 for $\eta_0 = 3$ Å, $\gamma = 1.3 \times 10^{-10}$Å.

Figure 3.4 demonstrates that by plugging parameters that we believe to be physically relevant into Equation 3.20, one can generate critical velocities that are on the order of those that have been found experimentally in past Quantum Fluids Laboratory experiments ($v_c \sim .01\frac{m}{s}$) [2]. It is interesting to note that there is a maximum in the critical velocity distribution which occurs at $q_{max} = \frac{1}{2\gamma_d}$, corresponding to the situation where the vortex core exactly encloses one half cycle of the oscillation of the substrate surface ($\lambda = 2\gamma_d$). When the core radius is much larger than the Fourier wavelength of the substrate surface, the vortex flow field sees an averaged surface that appears reasonably flat. Consequently, there are no sharp changes in geometry as seen from the vortex flow field, and the suction is minimal. As the Fourier wavelength shrinks to be of a size scale comparable to the core, the geometry of the surface has a much larger effect on the suction force generated. From Figure 3.2, we understand that the effective area of the surface that the core sees goes like $\frac{1}{cos[\theta]}$. This implies that the more rapid

the vertical change in geometry, the more area the vortex flow field "sees", and the more suction can be created as the amount of area being integrated over at large values of the vortex flow field increases. At $q_{max} = \frac{1}{2\gamma_d}$, the steepeness of the $\frac{1}{cos[\theta]}$ is maximized, and the suction force (critical velocity) is at a maximum. Finally, as the vortex core gets small compared to the Fourier wavelength, the substrate surface appears very flat locally around the core, and there are no extreme changes in geometry, which results in a reduced suction force.

Clearly the insight that this result provides about the details of the system relies on the premise that there is only one wavenumber present in the Fourier spectrum of the substrate. This is not true for any typical surface. An interesting point to note for future research, however, is the topic of monolayer self-assembly. Many recent advances in the field of supramolecular chemistry and self-assembly have enabled researchers to be able to pattern uniform monolayer surfaces with specifically tailored components. This point is particularly pertinent given the fact that our resonator substrate is gold-plated, and that there is a wealth of metal-thiol self-assembly chemistry available in the literature [14]. If one could control the exact properties of the substrate through self-assembly, and make the surface completely uniform, then one could perform very interesting studies on the pinning properties of a perfectly uniform surface, where all of the geometric, electronic, and magnetic properties of the surface would be completely known. This would eliminate many of the uncertainties that have been faced in the past in these types of studies. It is here that the formalism developed in this chapter could possibly find its greatest utility.

## 3.4 Summary

Ultimately, the derivation in this chapter was performed with the intent of developing a theoretical means of relating the geometrical properties of a substrate surface to the pinning force, or critical velocity, of a vortex on a defect site. While

it is impossible to analytically solve Equation 3.16 for a real substrate surface (although a statistical approach to the wavenumbers present in the frequency spectrum of the substrate could be implemented), it is instructive to use a simple complex exponential to qualitatively understand the effects of geometry on pinning strength. In essence, we can conclude that the more rapid the change in surface geometry in the region near to the core, the stronger the pinning force will be. This corroborates the generally accepted notion mentioned at the beginning of this chapter that geometrical defects provide energy minima that vortices are inclined to pin to. Theoretically, one could use Equation 3.16, and experimental results, to develop some knowledge of the frequency properties of a given substrate surface. This formalism also possesses important possible uses for a substrate surface that is geometrically uniform in a periodic sense, as in the situation of a self-assembled monolayer. Again, it is to be noted that considering the problem at hand in terms of the frequency properties of the substrate continues to be a useful methodology.

# Ch.4 Vortex Dynamics and Results

## 4.1 Vortex Precession and Relaxation

In Chapter 2, we developed an elementary model for vortex heating and calculated the resulting vortex dynamics. In this chapter, we use motivation from the models of Chapter 2, as well as from the idea of thinking in terms of the frequency properties of the substrate from Chapter 3, to develop a more rigorous means of modeling vortex interaction with the resonator substrate.

When a vortex tip drags across the substrate, Kelvin wave agitation is propagated up the core. The lowest wavenumber mode that can be propagated on the core is the quarter-wave precession corresponding to the boundary condition that the vortex core intersects the thin-film surface orthogonally (Figure 2.6). This corresponds to a quarter-wave Kelvin precession frequency of $\omega_{1/4}$ via Equation 2.8. We imagine a disturbance with this precession frequency, and the vortex continuing to be dragged along the defect-ridden substrate. In an unperturbed scenario, the vortex would be likely to pin to an energetically favorable geometrical defect; however, in the perturbed case the vortex core possesses agitation and has trouble doing so. Since the vortex tip is being dragged along the substrate, one can associate a frequency with the vortex dragging across the bumps on the substrate of $\omega_{interaction}$. This $\omega_{interaction}$ is essentially a measure of how frequently a vortex encounters a surface defect that propagates agitation up the core. If we model the surface very simply as a complex exponential as in Chapter 3, then there is only a single wavenumber needed to describe the substrate: $q_0$. If the vortex is moving at a velocity $v_v$, then we describe $\omega_{interaction}$ as:

$$\omega_{interaction} = q_0 v_v \tag{4.1}$$

Intuitively, whether or not the vortex is able to repin to a defect will be related to how frequently the vortex is being perturbed, compared to how fast that disturbance can propagate away from the defect site and the vortex can settle into an unagitated state again. If $\omega_{interaction} >> \omega_{1/4}$, then the vortex will have trouble pinning due to agitation extant on the core ($v_{c-hot} < v_{c-cold}$). On the other hand, if $\omega_{1/4} >> \omega_{interaction}$, then the vortex will easily repin to the substrate ($v_{c-hot} \approx v_{c-cold}$), as it will be able to "shake off" the agitation prior to the excitation of the next Kelvin wave. All conversation about the "ease of repinning" is, in more definite words, a conversation about the critical velocity of the vortex.

## 4.2 Steady-State Vortex Dynamics

We require a means of reducing the critical velocity of the vortex based on the essential time scales of the system described in the previous section. One of the simplest and most intuitive quantitative ways to describe the behavior we seek with a mathematical equation is the following expression that is common in dissipative systems:

$$v_{c-hot} = \frac{v_{c-cold}}{1+i\frac{\omega_{interaction}}{\omega_{1/4}}} \tag{4.2}$$

In utilizing Equation 4.2, we describe the reduction of the cold critical velocity as a relaxation process involving the disturbance on the core induced by the interaction of the vortex with the substrate. We use $\omega_{1/4}$ as a characteristic frequency scale associated with the lowest quarter wave precession of a Kelvin wave in order to provide an indication of the rate at which a disturbance propagates out of the core and the vortex relaxes back into an unperturbed state. Describing $\omega_{interaction}$ follows from Equation 4.1.

We seek to combine our new quantitative expression relating the time scales involved in the relaxation of the vortex to a reduction in the critical velocity. In

other words, we need to find a self-consistent solution with our previous equation describing quantized vortex motion, Equation 2.16. When Equation 4.2 and Equation 2.16 are solved simultaneously, one arrives at the scaled, analytic expression for the vortex velocity

$$\frac{v_v}{v_{c-cold}} = \frac{1}{\sqrt{2}\beta}\sqrt{\beta^2 v_s^2 - 1 + \sqrt{1 - 4\beta^2 + 2\beta^2 v_s^2 + \beta^4 v_s^4}}, \tag{4.3}$$

where $\beta = \frac{q_0 v_{c-cold}}{\omega_{1/4}}$. This expression contains all of the information in our model regarding the frequency properties of the substrate and the characteristic relaxation time of the Kelvin waves on the vortex core. It should be noted that $v_s$ is scaled to the critical velocity ($v_s \rightarrow \frac{v_s}{v_{c-cold}}$).

Similarly, one can deduce the expression for the scaled critical velocity as well:

$$\frac{v_c}{v_{c-cold}} = \frac{\sqrt{2}}{\sqrt{\beta^2 v_s^2 + 1 + \sqrt{1 - 4\beta^2 + 2\beta^2 v_s^2 + \beta^4 v_s^4}}} \tag{4.4}$$

The plots of these new expressions for the vortex velocity and the critical velocity appear in Figures 4.1 and 4.2, respectively.

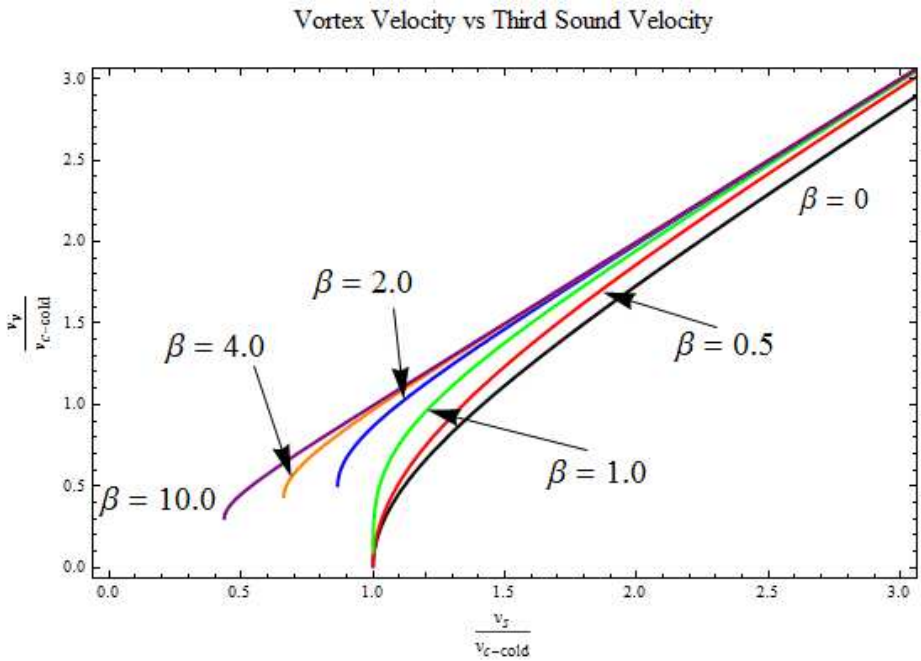


Figure 4.1 - Calculated scaled vortex velocity (Equation 4.3).

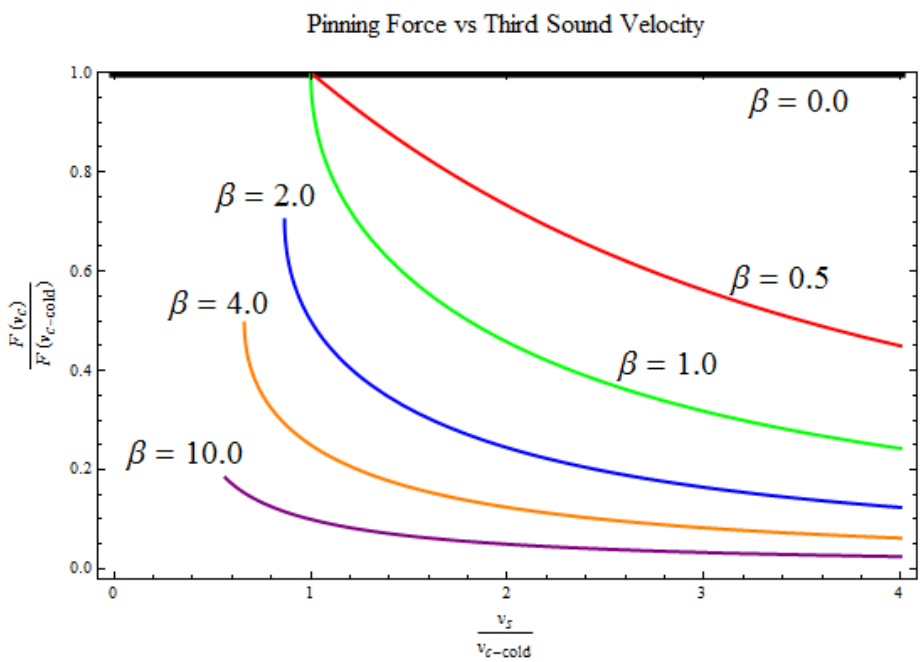


Figure 4.2 - Calculated scaled pinning force/critical velocity (Equation 4.4).

What is very interesting to note here is the similarity of the vortex velocity plot in Figure 4.1 to the qualitative behavior of the plots in Figures 2.7 and 2.8,

because it demonstrates that our two very different ways of modeling this system result in similar vortex dynamics. One does not need to be restricted to thinking purely in terms of reflected waves heating the core, or reductions in the slope as in Chapter 2, although both are instructive. One simply needs to imagine some type of agitation affecting the core that does not allow the vortex to pin as easily. In other words, the idea that some manifestation of excess kinetic energy on the vortex core results in a reduced pinning is the essential theme in all of these models, and in this chapter this concept takes the form of a time scale argument.

Again, there is the issue of solutions not existing for all $v_s$, which is a result of our solution being in the steady state, as in Chapter 2. Any region where the velocity of the vortex has no solution is a place where hysteresis will occur as the vortex is captured on a pinning site, as described previously in Section 2.4 and Figure 2.9.

## 4.3 Dynamic Drag Model

As mentioned previously, in 1991, Fred Ellis and Hai Luo published an article [15] that suggested that the critical velocity phenomena observed in free decays were the result of the pinning and unpinning of vortices from the resonator substrate. This process, they thought, was analogous to a classical friction force and could be modeled as such. We are ultimately interested in learning what the average power dissipated by a single vortex moving across the resonator substrate will be, because it is our hypothesis that dynamic vortex drag dissipation is the cause of these anomalous free decays. We assume that the frictional (drag) force acts opposite to the direction of the vortex motion, and that the average power dissipated can be described by:

$$P_{AV} = \frac{1}{T}\int_0^T \overrightarrow{f_{drag}} \cdot \overrightarrow{v_v} dt \tag{4.5}$$

where $T$ is the period of the third sound oscilllation, and the force, $\overrightarrow{\mathbf{f_{drag}}}$, is the pinning force that the vortex encounters as it drags across the substrate, described by:

$$\overrightarrow{f_{drag}} = \rho\kappa h_0 v_c \hat{v}_v \tag{4.6}$$

The difference between our model and calculations done previously, particularly in Anand Swaminathan's thesis, is that our modified model does not assume the critical velocity $v_c$, to be constant. Instead, we can replace $v_c$ by Equation 4.4, which describes how the critical velocity changes as a function of substrate properties $\beta$, and the background third sound flow, $v_s$. Similarly, we describe $v_v$ using our newly modified Equation 4.3.

Substituting in the corresponding expressions allows one to write Equation 4.5 as:

$$P_{AV} = \frac{\rho\kappa h_0 v_{c-cold}^2}{\sqrt{2}\beta^2}\frac{1}{T}\int_0^T \sqrt{2\beta^2 - \beta^2 v_s^2 - 1 + \sqrt{1 - 4\beta^2 + 2\beta^2 v_s^2 + \beta^4 v_s^4}}dt \tag{4.7}$$

We then choose to introduce the scaling $A = \frac{\eta}{\eta_c} = \frac{v}{v_{c-cold}}$. This greatly simplifies matters since all amplitudes can now be scaled to the critical point (kink point) amplitude, which can be read very easily from experimental data. A third sound cycle oscillation can be approximated by a simple sine function:

$$v_s(t) = A \cdot sin(\omega_{TS} t) \tag{4.8}$$

The average power dissipated by a single third sound cycle can be considered as consisting of two components. The first component of the drag dissipation can be thought of as the power dissipated from the time when the vortex depins from its cold critical velocity $v_{c-cold}$ to when the background superfluid flow reaches its peak. The second component is the drag dissipation associated with the time frame between the peak of the superfluid third sound cycle and the repinning of the vortex at the lower critical velocity, $v_{c-hot}$. The physics in both of these cycles is the same, and they are merely separated for the purpose of making the calculation simpler. The total power dissipated over a single third sound cycle can be determined by summing these components of the dissipation in the time average of Equation 4.5. These components are illustrated in Figure 4.3.

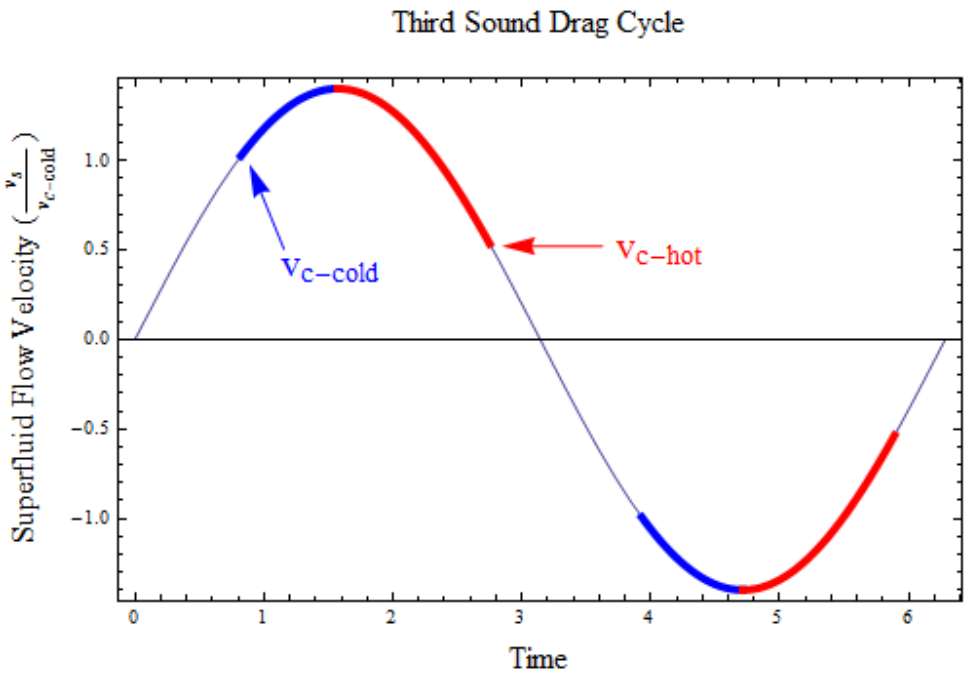


Figure 4.3 - Third Sound Flow Cycle. Superfluid flow velocity is scaled to the cold critical velocity. Blue denotes the dragging of the vortex from its depinning at $v_{c-cold}$ ($v_s = 1$ in the plot) to the peak. Red denotes the dragging of the vortex from the peak to $v_{c-hot}$ ($v_s < 1$ in the plot).

Using the scaling $\phi = \omega_{TS} t$ , one can write the full form of Equation 4.7 for the first component of the drag dissipation as

$$P_{AV} = \frac{\rho \kappa h_0 v_{c-cold}^2}{\pi} \int_{sin^{-1}[\frac{1}{A}]}^{\frac{\pi}{2}} \frac{1}{\sqrt{2}\beta^2} \sqrt{2\beta^2 - \beta^2 A^2 Sin^2[\phi] - 1 + \sqrt{1 - 4\beta^2 + 2\beta^2 A^2 Sin^2[\phi] + \beta^4 A^4 Sin^4[\phi]}} d\phi \tag{4.9}$$

and the second component similarly as

$$P_{AV} = \frac{\rho\kappa h_0 v_{c-cold}^2}{\pi}\int_{sin^{-1}[\frac{\mathbf{v_{c-hot}}}{A}]}^{\frac{\pi}{2}} \frac{1}{\sqrt{2}\beta^2}\sqrt{2\beta^2 - \beta^2 A^2 sin^2[\phi] - 1 + \sqrt{1 - 4\beta^2 + 2\beta^2 A^2 sin^2[\phi] + \beta^4 A^4 sin^4[\phi]}}d\phi \tag{4.10}$$

Equation 4.10 is dependent upon knowing exactly at what $v_{c-hot}$ the vortex will repin. Through some brief analysis, a closed form for determining the repinning critical velocity, $v_{c-hot}$ , solely as a function of $\beta$, can be determined from the previously mentioned equations, thereby making the bounds on the numerical integrals of 4.9 and 4.10 exact.

Prior to proceeding, it is useful to understand the effect of the $\beta$ term on the power dissipated by a single vortex. This information can be found in Figure 4.4, where we plot Equation 4.9 for different values of $\beta$. The total average power dissipated will be a sum of the contributions from Equations 4.9 and 4.10.

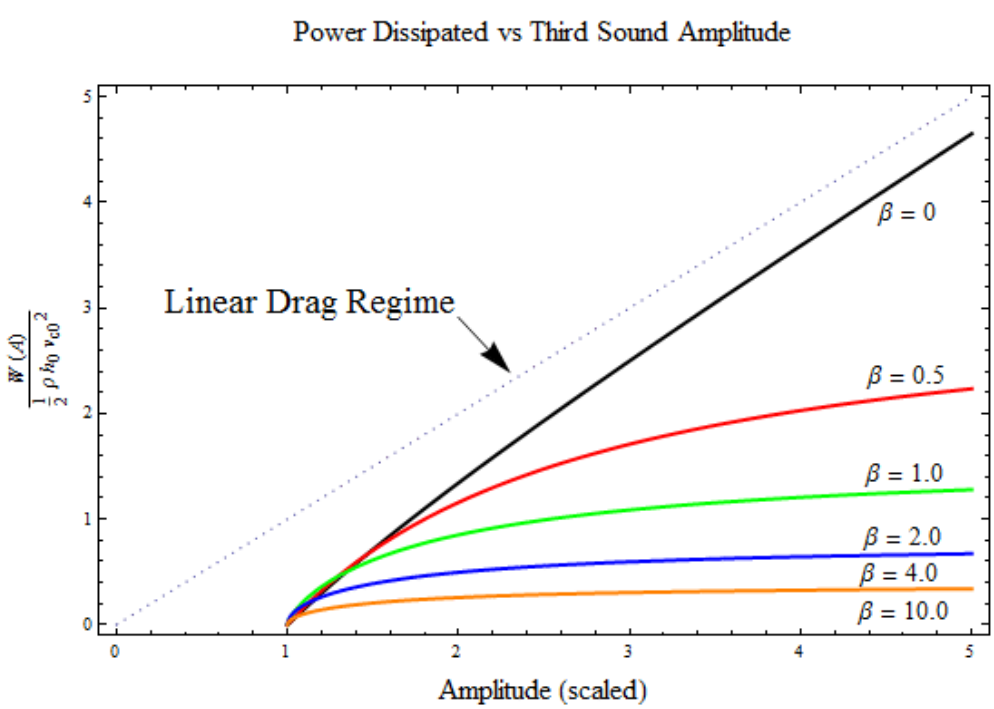


Figure 4.4 - Power dissipated by a single vortex as a function of the scaled third sound amplitude.

Figure 4.4 tells us that the $\beta$ parameter, which describes the agitation present on the core due to disruptive encounters with defects on the substrate, allows one to control the amount of energy a vortex dissipates as the third sound flow increases. A rather interesting point to note is that as one goes to higher amplitudes while at nonzero $\beta$, one does not recover the linear drag force type of behavior found in previous static drag models. This is undoubtedly due to the fact that while the vortex can dissipate energy for a longer duration if $\beta$ is nonzero, since it is unpinned and dragging for a longer period of time, the reduction in the critical velocity (pinning force) ultimately decreases the total amount of energy dissipated in a third sound oscillation. While this might limit the utility of this model since increasing $\beta$ by too much decreases the amount of energy a vortex can dissipate, ultimately we are only discussing one vortex. There are most likely more than just one vortex in our experimental system, so by increasing the number density of vortices in our model we can control the shape, and magnitude, of our power dissipation curve. This will in turn allow one to tailor the form of the free decay curve.

Since $P_{AV}$ is simply the average power dissipated by one vortex over one cycle of third sound flow, we define a total power dissipated:

$$W(A) = n \times P_{AV} \tag{4.11}$$

where $n$ is equal to the number density of vortices on the resonator substrate.

This $W(A)$ can be combined with the background exponential dissipation to produce the total energy lost in the wave

$$\frac{dE(A)}{dt} = -W(A) - \frac{\omega_0 E(A)}{2Q_0}, \tag{4.12}$$

where $\omega_0$ and $Q_0$ are associated with the drive frequency of the resonator and the background exponential dissipation in the system, respectively. $Q_0$ is chosen by fitting an exponential decay curve to the section of the free decay after the critical point.

$E(A)$ is the energy in the wave under the plane wave approximation, which is twice the kinetic energy, given by

$$E(A) = \tfrac{1}{2}\rho h_0 v_c^2 A^2 \tag{4.13}$$

Substituting this energy into Equation 4.12, its final form reads

$$\tfrac{dA}{d\tau} = -\tfrac{I(A)}{A} - \gamma A \tag{4.14}$$

where we use the scaling $\tau = \alpha t$, $\alpha = \frac{n\kappa}{\pi}$, $\gamma = \frac{\omega_0}{2Q_0}\frac{1}{\alpha}$, and $I(A)$ is a numerical integral corresponding to the scaled power dissipation associated with the sum of the two components of the drag dissipation, Equations 4.9 and 4.10. From dimensional analysis of Equation 4.14, it becomes clear that $\alpha$ is some type of rate constant and $\gamma$ is some type of scaled decay constant.

Equation 4.14 is a separable differential equation, so separating and integrating yields:

$$\tau = -\int_1^A \tfrac{A}{I(A)+\gamma A^2} dA \tag{4.15}$$

This equation can then be inverted to produce a decay amplitude $A$ as a function of $\tau$, and this is the method used to generate our theoretical decay curves.

In matching the experimental data to our model, we scale all of the experimental data such that the critical point (kink point) in the data corresponds to $\tau = 0$, with a critical amplitude of $A = 1$. We then scale our time axis by the value $\alpha$ associated with one of the fitting parameters of our model, $n$. Ultimately, there are four parameters that one can tune in order to get the best fit possible: $\beta$, $n$, $t_{crit}$, and $A_{crit}$, where $t_{crit}$ and $A_{crit}$ represent the critical time and amplitude chosen by hand from the experimental data set. As one can see from Figure 4.5, $A_{crit}$ is an easier parameter to place precisely than $t_{crit}$, as there is some ambiguity as to the exact point of the critical time. Therefore, we fix $A_{crit}$ and use a three parameter model, allowing $t_{crit}$ to be floated in the range just around the critical point that allows for the best fit, since the exact time is hard to pin down. It should be noted that we fit by finding the smallest least-squares value by hand since there was not adequate time to devise a least-squares fitting routine, however the most precise results should involve an automated fitting routine. It should also be noted that $I(A)$ was fit to a linear combination of polynomials in order to allow for a closed form of the integrand that could be evaluated more quickly with computational software.

As mentioned in Chapter 1, the model used in Anand's thesis could not adequately describe both the curvature of the decay curve and the position of the critical point simultaneously. This is shown in greater detail in Figure 4.5, where we see the fits resulting from the static frictional drag force ($\beta = 0$) in Anand Swaminathan's thesis.

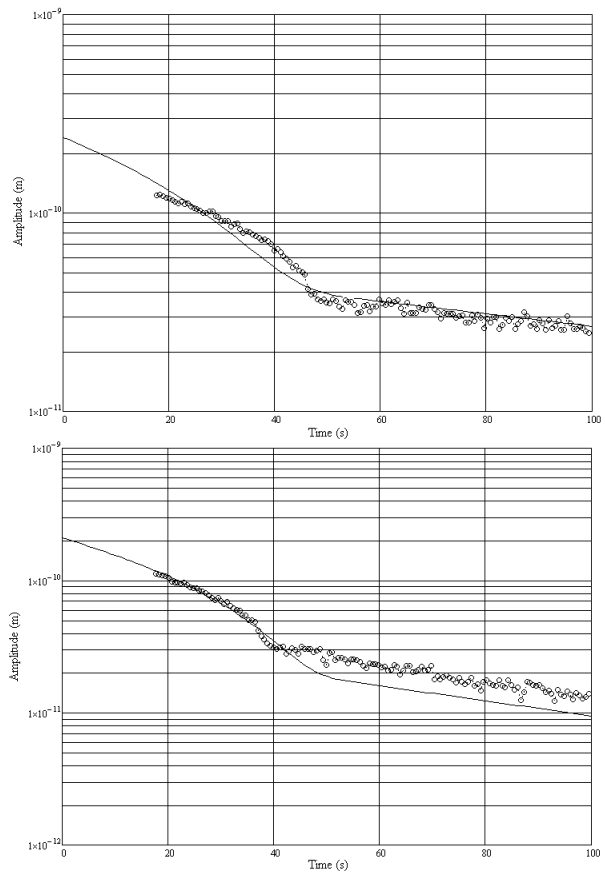


Figure 4.5 - Decay curve results from Anand Swaminathan's thesis [2]. There is an inability to simultaneously match the curvature of the decay amplitude and the critical point position.

The new results corresponding to the incorporation of the $\beta$ parameter are presented in Figure 4.6, where we fit a respresentative experimental free decay curve.

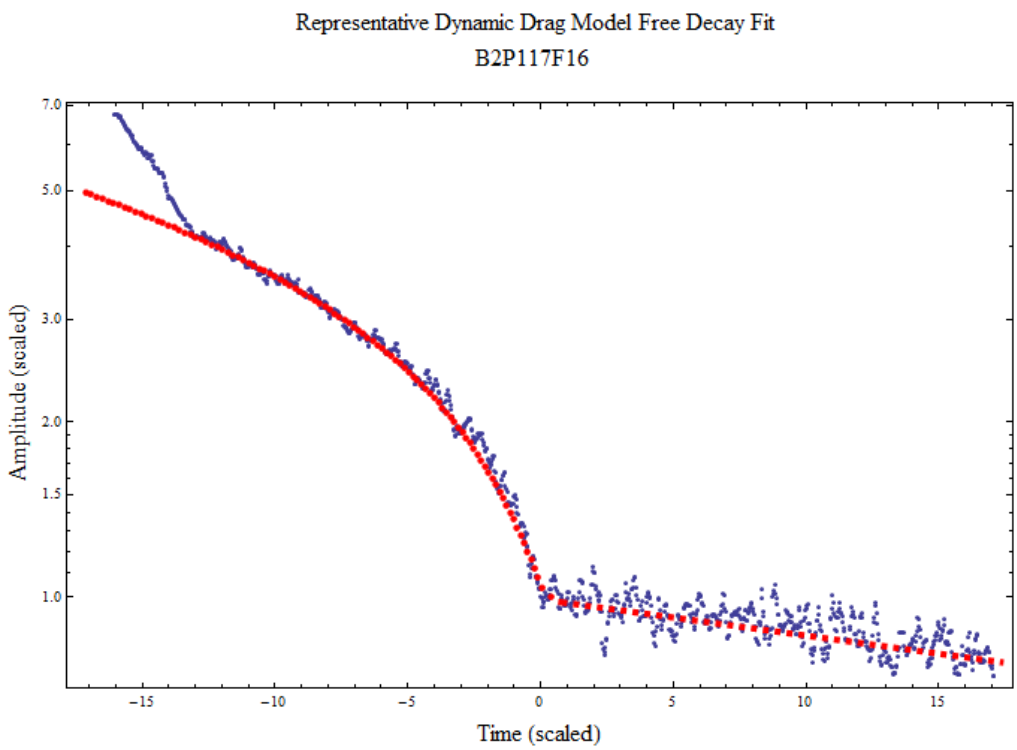


Figure 4.6 - Decay curve fit resulting from the dynamic drag model. Note a remarkably better ability to simultaneously match the curvature of the decay curve and the position of the critical point.

Clearly, this results in an improved fit to the experimental free decay data. In the analysis done in Anand Swaminathan's thesis there was ultimately only a single parameter that could be tuned in these fittings: the number density of vortices on the substrate. Each vortex had a specific dissipation function that could not be altered. By incorporating this $\beta$ term that involves the interaction of the vortex with the substrate, we now have a means of tuning the amount of power dissipated by each vortex. This results in a better fit of the experimental data.

Fits for the range of experimental data sets that we have available have $\beta$ ranging between .5 and 5, and $n$ ranging between $2 \cdot 10^6 \frac{1}{m^2}$ and $5 \cdot 10^7 \frac{1}{m^2}$. The experimental apparatus used has a total surface area of 1 cm$^2$, which corresponds to between $2 \cdot 10^2$ and $5 \cdot 10^3$ vortices present on our resonator surface in a given

experiment. This is well below the theoretical limit for vortex density, which corresponds to dividing the resonator surface area by the vortex core area.

An interesting phenomenon in fitting the data is that equally good fits can be found for many values of $\beta$ and $n$. This was at first unnerving, as it implied that there were not fitting values unique to the physical situation. However, after some analysis we found that if one takes the ratio of $\frac{\beta}{n}$ for all of the values of $\beta$ and $n$ that result in good fits of a particular data set, that ratio will always be constant. This implies that there is some interaction per vortex that is characteristic of a given experimental system, and thus $\frac{\beta}{n}$ is the parameter of physical importance. The important physics that happens occurs when one changes $\beta$ from 0 to the lowest value that allows for an accurate fit, implying that an amount of interaction per vortex has been reached that is characteristic of the system. Changing $\beta$ and $n$ to get good fits after that point reveals no new information about the system.

While there is some slight discrepancy between the exact form of the curves (the curvature of the decay amplitude just above the critical point is very slightly mismatched), this new model of dynamic vortex drag allows one to simultaneously fit the curvature of the decay amplitude and the exact location of the critical point dramatically better than the previous static drag force model presented in Figure 4.5. It is important to note that we see this kind of accuracy in fits over a range of data sets, which further supports the proposition of dynamic vortex drag. Other fits are not included in this thesis because qualitatively they are identical to the fit found in Figure 4.6, and would not provide any more useful information to the reader. This thesis serves as an initial survey of the concept of dynamic vortex drag and is not meant as an in-depth analysis of the experimental data we have available, although that could prove to be an interesting future project

## 4.4 Summary

Our studies allow us to conclude that dynamic vortex interaction is indeed a physical phenomenon that must be considered when modeling quantized vortex dynamics in thin-film superfluid $^4$He systems. Our incorporation of the $\beta$ parameter results in remarkably better fits of experimental data that has for many years been unable to be reconciled with theory. While the previous theoretical models of Chapter 2 allowed us to produce vortex velocity curves very similar to those found in this chapter, ultimately our current model is superior because it presents a more rigorous basis for discussing vortex dynamics involving interactions with the substrate, and also provides closed forms of the vortex velocity and critical velocity equations that allow us to more easily calculate theoretical free decay curves. While reflection coefficients and actual "heating" is a simple way to think of vortex interaction intuitively, ultimately the many ways we have presented vortex interaction can be nicely summed up in the $\beta$ term we have presented in this chapter, which simply makes arguments based on the time scales associated with the agitation and relaxation of the vortex.

# Ch.5 Conclusion

## 5.1 Dynamic Vortex Drag

Through our various simulations we have deduced that incorporating dynamic vortex drag into our various models helps account for many of the deficiences of the static drag model. What precisely produces this *dynamic* vortex drag does not need to be specified, but we know that it is some kind of wave motion on the vortex core induced by the pinning and unpinning of the vortex on substrate defect sites, which results in a retained, nonzero kinetic energy on the core. Quantized vortex cores are known to be capable of sustaining wave modes, particularly Kelvin wave modes, and thus we believe that these are the wave modes responsible for this dynamic interaction with the substrate. Whether we model this agitation as a heating associated with a core reflection coefficient, a physical distortion resulting in a change in the geometry of the vortex that leads to reduced pinning, or simply as a time scale argument based on the interaction of the vortex with the substrate, we arrive at similar dynamical results involving vortex motion and reduced pinning. It is therefore important to not lock oneself into thinking of this depinning in any one particular way, but more as a general agitation on the core.

Using our dynamic drag model, we determine that there are between 200 and 5,000 vortices present on the resonator surface in any given experiment. We have also learned that $\frac{\beta}{n}$, the interaction per vortex, is the important physical paramater of our model to be considered in future studies.

## 5.2 Quantum Swirling

Previous studies have been performed examining the quantum swirling of vortices on the resonator substrate [16]. In these experiments, there were found to be distributions of vortices present at different radii away from the resonator center. However, in all studies there was found to be an unexpected number of vortices clumped near the center of the resonator. This was thought to be the result of many vortices being generated over the entire resonator, and then pushed into the middle as a result of the Magnus force acting on them during the third sound flows. When trying to model this center-heavy distribution, there was a failure in matching experimental data. The static friction drag model was incapable of explaining the extent of the clumping of vortices near the center of the resonator cell. Dynamic vortex drag could serve as a possible explanation for this phenomenon.

In the dynamic vortex drag model, the vortex pinning force is reduced as the vortex drags along the substrate. If the pinning force is reduced, then it will be easier for these vortices to move along the substrate, allowing them to be pushed closer to the middle of the resonator. This could, in turn, possibly explain the clumping of vortices near the middle of the resonator cell. While there are many details to be worked out in this proposition of a solution to the quantum swirling problem, it is the logical next step in validating the theory of dynamic vortex drag using other experiments performed in the Quantum Fluids Laboratory.

## 5.3 Conclusion

This thesis set out to determine whether or not the proposition of dynamic vortex drag resulting from Kelvin wave excitations on a vortex core could help explain heretofore unreconciled anomalous free decay data. We have implemented dynamic vortex drag in many different forms, and have discovered that all of the implementations are potentially capable of explaining phenomena that the static

drag model has failed at describing. The most sophisticated implementation found in Chapter 4 showed itself to be capable of precisely fitting and explaining anomalous free decay data that have not been explained previously. We thus conclude from our studies that dynamic vortex drag is very likely an important physical phenomenon to be considered in thin-film superfluid $^4$He systems. The next logical step in the application of the dynamic drag model is in attempting to explain quantum swirling phenomena described in the previous section, as an effective application of this model to an entirely different experimental phenomenon would help to put the proposition of dynamic vortex drag on solid ground.

# Appendix A - A Generic Fourier Problem

Given the boundary condition x(t) on the vortex core tip, find the function y(t) in the expression below using only the slow branch of the dispersion relation, i.e. neglect all negative frequencies (frequencies that travel with the circulation) in the Fourier Analysis

$$x(t) + iy(t) = 2\frac{1}{\sqrt{2\pi}} \int_0^\infty g(\omega) \cdot e^{-i\omega \cdot t} d\omega \tag{A.1}$$

where

$$g(\omega) = \frac{1}{\sqrt{2\pi}} \int_0^\infty x(t) \cdot e^{i\omega \cdot t} dt \tag{A.2}$$

Use a carefully defined $\theta$ function (step function):

$$x(t) + iy(t) = 2\frac{1}{\sqrt{2\pi}} \int_{-\infty}^\infty \theta(\omega) g(\omega) e^{-i\omega \cdot t} d\omega \tag{A.3}$$

with

$$\theta(\omega) = \frac{1}{2\pi i} \int_{-\infty}^\infty \frac{e^{i\omega \cdot t}}{t - \imath\lambda} dt \ \lambda \to 0 + \varepsilon \tag{A.4}$$

Substitute all known expressions

$$x(t)+iy(t)=2\frac{1}{\sqrt{2\pi}}\int_{-\infty}^{\infty}\left(\frac{1}{2\pi i}\int_{-\infty}^{\infty}\frac{e^{i\omega\cdot s}}{s-i\lambda}ds\right)\left(\frac{1}{\sqrt{2\pi}}\int_{-\infty}^{\infty}x(u)e^{i\omega\cdot u}du\right)e^{-i\omega\cdot t}d\omega\ \lambda\leftarrow 0+\varepsilon \quad \text{(A.5)}$$

Use the expression

$$\int_{-\infty}^{\infty}e^{i(s+u-t)\omega}d\omega=2\pi\delta(s+u-t) \quad \text{(A.6)}$$

$$x(t)+i\cdot y(t)=\frac{1}{i\omega}\int_{-\infty}^{\infty}\frac{x(t-s)}{s-i\lambda}ds\ \lambda\rightarrow 0+\varepsilon \quad \text{(A.7)}$$

Proceed by carefully evaluating the limit:

$$x(t)+iy(t)=\frac{1}{i\omega}\int_{-\infty}^{\infty}x(t-s)\frac{s+i\lambda}{s^2+\lambda^2}ds=x(t)-\frac{i}{\pi}\int_{-\infty}^{\infty}x(t-s)\frac{s}{s^2+\lambda^2}ds\ \lambda\leftarrow 0$$

(A.8)

Resulting in the final expression for y(t)

$$y(t)=\frac{1}{\pi}\int_{-\infty}^{\infty}x(t-s)\frac{s}{s^2+\lambda^2}ds\ \lambda\leftarrow 0 \quad \text{(A.9)}$$

**Gaussian Example**

$$x(t)=\frac{A}{\sqrt{2\pi\sigma^2}}e^{-\frac{1}{2}\left(\frac{t}{\sigma}\right)^2}$$

Evaluate y(t):

$$y(t) = -\frac{1}{\pi}\int_{-\infty}^{\infty} \frac{A}{\sqrt{2\pi\sigma^2}} e^{-\frac{1}{2}\left(\frac{t-s}{\sigma}\right)^2} \frac{1}{s} ds$$

Evaluating this integral via Mathematica yields

$$y(t) = -\frac{A}{\sqrt{2\pi\sigma^2}} e^{-\frac{1}{2}\left(\frac{t}{\sigma}\right)^2} erfi\left(\frac{t}{\sigma\sqrt{2}}\right)$$

where

$$erfi\,(x) = \frac{2}{\sqrt{\pi}}\int_0^x e^{u^2} du$$

which can be used to evaluate the y(t) associated with a Gaussian x(t) boundary condition in time.

# Appendix B - Geometrical Reflection Coefficient

In this appendix we attempt to describe the reflection and transmission process associated with a traveling wave reflecting off of a superfluid film vortex surface. This argument is purely geometrical and includes none of the hydrodynamic details of the system.

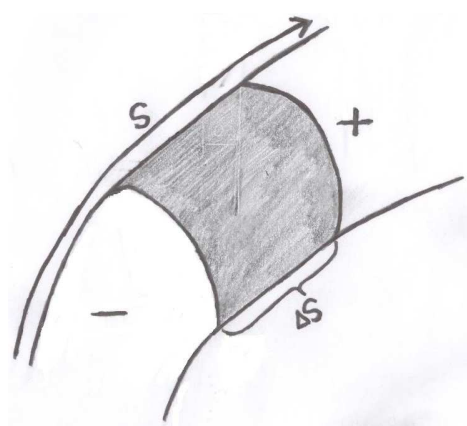


Figure B.1 - Force balancing on a differential section of the vortex core.

We begin by force balancing with Newton's Second Law in the radial component of the vortex core

$$\frac{\partial v_r}{\partial t} = \frac{(P_- - P_+)\cdot A}{M} = \frac{\rho g(n_- - n_+)d\phi R(s)h}{\rho d\phi R(s)h\cdot\triangle s} = \frac{g(n_- - n_+)}{\triangle s} = -g\frac{\partial \eta}{\partial s} \tag{B.1}$$

Now doing the same thing in the $\phi$ component:

$$\frac{\partial v_\phi}{\partial t} = \frac{(P_- - P_+)\cdot A}{M} = \frac{\rho g(n_- - n_+)d\phi h\triangle s}{\rho d\phi R(s)h\triangle s} = \frac{-g}{R(s)}\frac{\partial \eta}{\partial \phi} \tag{B.2}$$

Next we can balance the volume flow rate in the system:

$$Area \cdot \frac{\partial \eta}{\partial t} = \dot{v}_- - \dot{v}_+ = (v_r(d\phi R(s)h))^- - (v_r(d\phi R(s)h))^+ + (v_\phi hds)^- - (v_\phi hds)^+ \tag{B.3}$$

Where the area is simply equal to $d\phi R(s)ds$.

Rewriting B.3, we can arrive at the relation

$$\frac{\partial \eta}{\partial t} = \frac{-h}{R(s)} \left[ \frac{\partial}{\partial s}(R(s)v_r) + \frac{\partial v_\phi}{\partial \phi} \right] \tag{B.4}$$

Since these are traveling waves, they take the standard form of

$$x(t) = e^{i(m\phi - \omega t)} \tag{B.5}$$

So we can integrate Equations B.1, B.2, and B.4 and combine them to arrive at the expression

$$-i\omega\eta = \frac{-h}{R(s)} \left[ \frac{\partial}{\partial s}(R(s)\frac{g}{i\omega}\frac{\partial \eta}{\partial s}) + im(\frac{m}{\omega}\frac{g}{R(s)}\eta) \right] \tag{B.6}$$

Assuming that g has no s dependence, one can rewrite Equation B.6 in the following form

$$\frac{\partial^2 \eta}{\partial s^2} + \frac{R'(s)}{R(s)}\frac{\partial \eta}{\partial s} + \left( k^2 - \frac{m^2}{R(s)^2} \right) \eta = 0 \tag{B.7}$$

where $k^2 = \frac{\omega^2}{gh}$. Using the relation that

$$k^2 = q_0^2 - \frac{m^2}{a^2} \tag{B.8}$$

and assuming letting $a = 1$, we can write down the final form of the differential equation describing the dynamics of our system:

$$\frac{\partial^2 \eta}{\partial s^2} + \frac{R'(s)}{R(s)}\frac{\partial \eta}{\partial s} + \left(q_0^2 + m^2(1 - \frac{m^2}{R(s)^2})\right)\eta = 0 \tag{B.9}$$

Equation B.9 is the differential equation that governs the dynamics of the system for an arbitrary geometry, R(s).

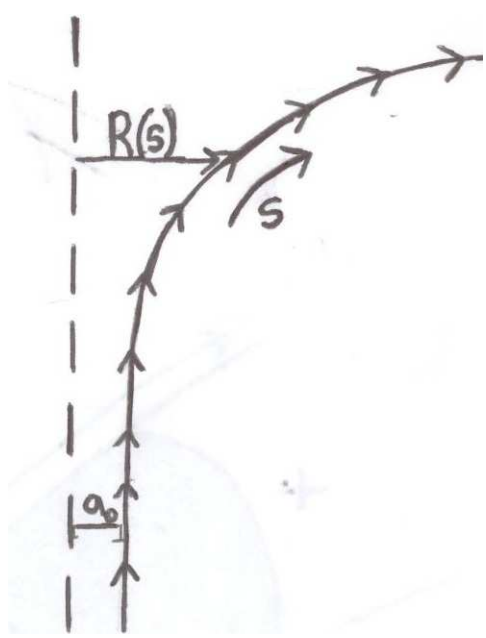


Figure B.2 - R(s) vs s for a given vortex core.

We wish to know the solution to this equation along the whole extent of the core. We are already aware of what the solutions are to the surface waves at large

s values. They are given by traveling Bessel Functions, but for $s >> m$, reduce down to the form

$$\eta(s) = \frac{e^{iks}}{\sqrt{ks}} \tag{B.10}$$

Equation B.9 is construcucted specifically so that when s gets very negative, (i.e. the core radius is constant), you essentially just have simple harmonic motion on the core. Since we wish to know the amplitudes, and not just the types, of waves associated with this system, we use 4th order Runge-Kutta numerical integration to develop a solution to $\eta(s)$ for all s.

Once the solution to $\eta(s)$ is known for all s, or more importantly at the surface of the vortex and on the straight core length, one can then go about determining a reflection coefficient through a comparison of the amplitudes of the incoming (core) and outgoing (surface) waves through simple complex analysis. A simple means of doing this is by plotting the real and imaginary components of $\eta(s)$ on the x and y axis, respectively. If there is no reflection, then plotting the data this way should result in a perfect circle, because the amplitude of the wave has not been influenced by the geometry of the vortex. However, if reflection does occur, then the data should show the circle deforming into an ellipse, where one can determine information regarding the reflection coefficients from the length of the major and minor axes of the ellipse.

# Bibliography


[1] David R. Tilley and John Tilley. *Superfluidity and Superconductivity.* Halsted Press, New York, 1974.

[2] Anand Swaminathan. *Vortex Dissipation in Superfluid Third Sound Flows.* Undergraduate Honors Thesis, Wesleyan University, Middletown, CT, 2009.

[3] Russel J. Donnelly. *Quantized Vortices in Helium II.* Cambridge Studies in Low Temperature Physics. Cambridge University Press, Cambridge, 1991.

[4] Ian Carbone. *Steady State and Transient Third Sound Behavior.* Undergraduate Honors Thesis, Wesleyan University, Middletown, CT, 2006.

[5] K.W. Schwarz. "Three-dimensional vortex dynamics in superfluid$^4$He : Line-line and line-boundary interactions". *Physics Review B,* 31:5782-5804, 1985.

[6] L. Hough L.A.K. Donev and R.J. Zieve. "Depinning of a superfluid vortex line by Kelvin waves". *Physics Review B,* 64:180512-180516, 2001.

[7] W. Thomson, Philos. Mag. 10, 155 (1880); J.J. Thomson, A Treatise on the Motion of Vortex Rings (Macmillan, London, 1883).

[8] C.F. Barenghi R.Hanninen and M. Tsubota. "Anomalous translational velocity of vortex ring with finite-amplitude Kelvin waves". *Physical Review E*, 74:046303-046303-5, 2006.

[9] W.F. Vinen M. Tsubota and A. Mitani. "Kelvin-Wave Cascade on a Vortex in Superfluid $^4$He at a Very Low Temperature". *Physical Review Letters,* 91: 135301-135301-4, 2003.

[10] Shoji Fujiyama Risto Hanninen and Makoto Tsubota, "Vortex Pinning to a Solid Sphere in Helium II", *J Low Temp Phys*, 148:263-267, 2007.

[11] Oliver Ryan. *Vortices in Liquid Helium.* Undergraduate Honors Thesis, Wesleyan University, Middletown, CT, 1992.

[12] F. M. Ellis and C. Wilson. "Excitation and Relaxation of Film Flow Induced by Third Sound", J. Low Temp. Phys., 113, 411 1998.

[13] Charles Kittel. *Introduction to Solid State Physics,* 8th Edition, Wiley, 2004.

[14] Love et al.; Estroff, Lara A.; Kriebel, Jennah K.; Nuzzo, Ralph G.; Whitesides, George M. "Self-Assembled Monolayers of Thiolates on Metals as a Form of Nanotechnology". Chem. Rev. 105 (4): 1103–1170. 2005

[15] F. M. Ellis and H. Luo. "Low Temperature Exponential and Linear Free Decay of Third Sound Resonances", Physica, B169, 521 (1991).

[16] Crista Wilson. *Swirling Superfluid* $^4$He *Films.* Ph.D Thesis, Wesleyan University, Middletown, CT, 1998.